Sánchez-Monreal, J., García-Salaberri, P. A. & Vera, M. (2017). A genetically optimized kinetic model for ethanol electro-oxidation on Pt-based binary catalysts used in direct ethanol fuel cells. *Journal of Power Sources, 363*, 341–355.

DOI: 10.1016/j.jpowsour.2017.07.069

A genetically optimized kinetic model for ethanol electro-oxidation on Pt-based binary catalysts used in direct ethanol fuel cells

Juan Sánchez-Monreal, Pablo A. García-Salaberri, Marcos Vera*

Dept. de Ingeniería Térmica y de Fluidos, Universidad Carlos III de Madrid, 28911 Leganés, Spain

Abstract

A one-dimensional model is proposed for the anode of a liquid-feed direct ethanol fuel cell. The complex kinetics of the ethanol electro-oxidation reaction is described using a multi-step reaction mechanism that considers free and adsorbed intermediate species on Pt-based binary catalysts. The adsorbed species are modeled using coverage factors to account for the blockage of the active reaction sites on the catalyst surface. The reaction rates are described by Butler-Volmer equations that are coupled to a one-dimensional mass transport model which incorporates the effect of ethanol and acetaldehyde crossover. The proposed kinetic model circumvents the acetaldehyde bottleneck effect observed in previous studies by incorporating CH_3CHOH_{ads} among the adsorbed intermediates. A multi-objetive genetic algorithm is used to determine the reaction constants using anode polarization and product selectivity data obtained from the literature. By adjusting the reaction constants using the methodology developed here, different catalyst layers could be modeled and their selectivities could be successfully reproduced.

Keywords: DEFC modeling, ethanol electro-oxidation, reaction mechanism, coverage factors, product selectivity, genetic optimization

1. Introduction

Direct alcohol fuel cells (DAFC) represent a potential alternative to the archetypical hydrogen-fed polymer exchange membrane fuel cell (PEMFC) for two main reasons: the ease of production, storage, and delivery of liquid alcohols (e.g., methanol, ethanol, ethylene glycol, n–propanol, etc.), and their higher volumetric energy density compared to hydrogen [1]. This makes them suitable power sources for portable electronic devices such as cell phones, laptop computers, or military equipment. In contrast,

*Corresponding author. Tel.: +34-916249987; fax: +34-916249430.
Email address: marcos.vera@uc3m.es (Marcos Vera)
URL: http://fluidosuc3m.es/people/mvcoello (Marcos Vera)

DAFCs have two major drawbacks: the sluggish kinetics of the alcohol electro-oxidation reaction and the crossover of alcohol and water from anode to cathode through the polymeric membrane [2–5].

Among various alcohols, methanol is the most used due to its high energy density and relatively fast electro-oxidation kinetics. However, it has several drawbacks: it is easily flammable, highly volatile (boiling point 65°C), and relatively toxic, which may lead to environmental problems due to its large miscibility with water. Moreover, it is not fully renewable, as it is typically produced from gaseous hydrocarbons or synthesis gas (i.e., H_2 + CO) obtained by the partial oxidation of a hydrocarbonaceous feed. Ethanol offers an interesting alternative because it can be readily produced by fermentation of biomass, including agricultural raw materials, and is much less toxic [3, 6]. Furthermore, its diffusivity in polymeric membranes is smaller than that of methanol, which together with its sluggish electrochemical oxidation kinetics produces a lesser effect on the cathode performance [7, 8]. On top of that, its mass energy density is about 30% larger than that of methanol, and it is already the major renewable biofuel. For instance, countries like Brazil have already deployed a strong ethanol distribution network in petrol stations [9].

Nowever, the ethanol oxidation reaction (EOR) is slower and significantly more complex than the methanol oxidation reaction. The EOR proceeds through a multi-step reaction process that involves adsorbed species like acetyl (CH_3CO_{ads}) and carbon monoxide (CO_{ads}), and leads to a variety of oxidation products such as acetaldehyde (CH_3CHO), acetic acid (CH_3COOH), carbon dioxide (CO_2), and methane (CH_4) [4, 10–19], and in smaller amounts ethyl acetate, ethane, ethylene glycol, formic acid and others [12, 20–22]. The major oxidation products of ethanol on Pt electrodes are indeed acetaldehyde and acetic acid, not carbon dioxide [23], making the incomplete oxidation of ethanol one of the main unresolved problems in direct ethanol fuel cells (DEFC). It has been found that the main reason for the low CO_2 selectivity is related to the C–C bond cleavage due to the blocking effect of the surface oxidant [24, 25] and that the sp^2 bond is less susceptible to react [25, 26]. Binary catalysts, such as Pt–Sn and Pt–Ru, exhibit a larger activity for the EOR compared to pure Pt electrodes [19, 20, 24–33]. In this case, the blockage of the active sites is partially mitigated via a bifunctional mechanism that allows the adsorption of hydroxyl groups at lower potentials on the secondary metal, thus favoring the further oxidation of the Pt-adsorbates that block the active catalyst sites [34–36].

Another problem that hinders DEFC operation is the permeation of ethanol from anode to cathode, which leads to the parasitic electro-oxidation of ethanol at the cathode catalyst. The negative effects of ethanol crossover include cathode depolarization, poisoning of the cathode catalyst by the permeated ethanol and its intermediate oxidation products, and reduced fuel utilization [16, 37–39]. These phenom-

ena result in a reduction of the overall system efficiency, which is particularly pronounced at low current densities and high ethanol concentrations.

Regarding the modeling activity, most early DEFC models assumed the complete oxidation of ethanol to CO_2 with the transfer of 12 electrons [40, 41]. Other models considered the oxidation of ethanol to acetic acid with the transfer of only 4 electrons [42–44]. It was not until recently that DEFC models started to account for the complex multi-step kinetics of the EOR [18, 45, 46], including the effect of intermediate species such as acetic acid and acetaldehyde [10]. These models typically involve the calculation of the coverage factors of the intermediate species adsorbed on the catalyst layers (CL) [47], an approach also used in direct methanol fuel cell (DMFC) modeling [48–51]. In a recent work, Meyer et al. [18] proposed a branched reaction mechanism that involved different electron transfers depending on the pathway. Despite the good agreement in terms of polarization curves, the composition of the products predicted with this model is far from satisfactory, as recently shown by the authors [52].

Due to the importance of crossover in DEFC performance, most models have also included this effect [18, 39–45, 51]. Since the molecular structures of ethanol and methanol are very similar, all crossover models for ethanol are based on those previously developed for methanol [53], with the crossover flux driven by molecular diffusion and electro-osmotic drag. By contrast, the crossover of free intermediate species such as acetaldehyde or acetic acid has not been fully addressed, except by Meyer et al. [18]. Interestingly enough, even when ethanol crossover is considered, only a few models account for the mixed potential at the cathode due the parasitic electro-oxidation of ethanol. The crossover of oxygen from cathode to anode, with the associated mixed potential at the anode, represents another source of potential losses in DEFCs that has only been recently addressed [4, 22].

The aim of this paper is to develop a one-dimensional (1D) across-the-channel model for the anode of a DEFC accounting for the complex multi-step character of the EOR. The reaction mechanism, which considers free and adsorbed intermediate species on a Pt-based binary catalyst, represents an extension of the mechanism recently proposed by Meyer et al. [18]. As main novelty, the improved mechanism incorporates the production of acetic acid from ethanol via CH_3CHOH_{ads}, which is now explicitly considered among the adsorbed intermediates, and a genetic algorithm is used to select the reaction constants so as to enhance the predictive capabilities (including both anode overpotential and product selectivity) at the full current density range.

The structure of the paper is as follows. The mathematical model is presented first; including the description of the model assumptions, the physical domain, and of full set of equations. These include the multi-step description of the EOR at the anode catalyst, the mass transport of the free species at

the anode gas diffusion layer, and ethanol and acetaldehyde crossover. Illustrative numerical results are presented next, with special emphasis on the validation of the model against experimental results and a discussion of the agreements and disagreements. The concluding remarks are presented in the last section.

2. Model assumptions and physical domain

2.1. Model assumptions

In the development of the mathematical model, a number of simplifying assumptions have been made: *i*) the cell operates in steady-state; *ii*) the cell temperature (T) is uniform; *iii*) the concentrations of ethanol (E), acetaldehyde (A), and acetic acid (AA) are sufficiently small for the liquid phase to be considered a diluted aqueous solution; *iv*) the membrane (assumed to be Nafion® 117) is fully hydrated and is impermeable to gases; *v*) the ohmic losses in the catalyst layers, gas diffusion layers, and bipolar plates are considered negligible compared to ohmic losses in the membrane; *vi*) the overpotentials, coverage factors, and free species concentrations are constant across the catalyst layers; *vii*) the catalyst layer consists of a Pt-based binary catalysts that allows the adsorption of hydroxyl groups at lower potentials on the secondary metal according to the bifunctional mechanism described in [34–36]. Although some of this assumptions could be easily revised to incorporate additional effects in future work, they will be maintained here for simplicity.

2.2. Physical domain

Figure 1 shows a schematic representation of a DEFC. The cell is divided into seven regions: anode channel (ac); anode gas diffusion layer (agdl); anode catalyst layer (acl); polymeric membrane (mem); cathode catalyst layer (ccl); cathode gas diffusion layer (cgdl); and cathode channel (cc). In the 1D across-the-channel anode model presented in this work only the anode gas diffusion layer (agdl), the anode catalyst layer (acl), and the membrane (mem) are included. The figure also shows the notation used for the concentrations of the free species at the anode/cathode channels, and for the thickness of the different layers of the membrane electrode assembly (MEA).

3. Anode one-dimensional model

3.1. Anode catalyst layer.

Different reaction mechanisms have been proposed in the literature for the EOR [20, 24, 25, 54, 55]. Due to the large amount of intermediate species, both free and adsorbed, and of potential elementary

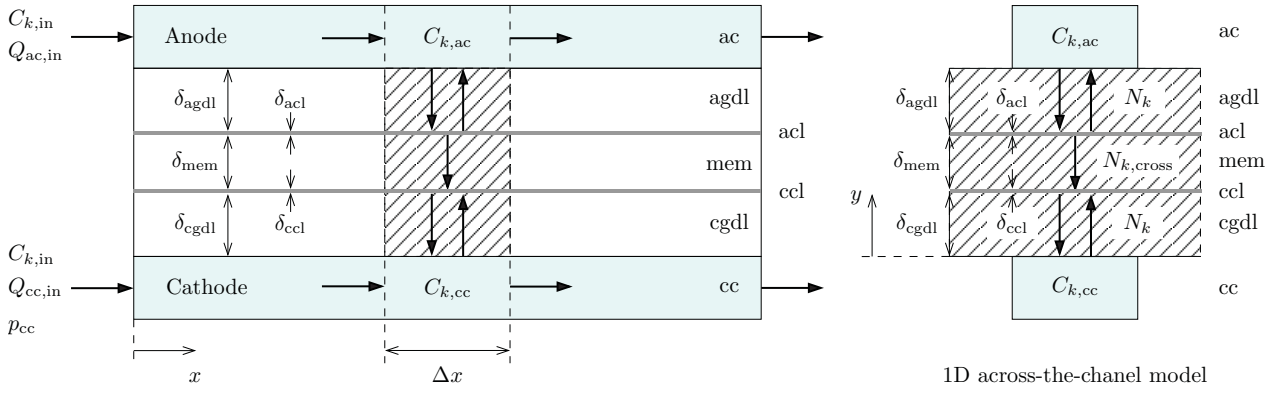

Figure 1: Schematic representation showing the different regions of a DEFC and highlighting the physical domain covered by the 1D across-the-channel model. The figure summarizes the notation used for the channel concentrations, $C_{k,\mathrm{ac/cc}}$, the molar fluxes across the porous layers, N_k, and the membrane crossover flux, $N_{k,\mathrm{cross}}$, of free species, k, as well as the thickness of the different layers of the MEA (δ_ℓ, ℓ = agdl, acl, mem, ccl, cgdl). Left: side view; right: cross-sectional view.

reactions, mathematical models exhibit different levels of complexity in the description of the EOR multi-step reaction [18, 45, 46]. Figure 2 shows the kinetic model proposed in this work. The different elementary reactions considered are listed in Table 1. The mechanism involves five adsorbed species, four of them attached to the Pt-sites (CH_3CHOH_{ads}, CH_3CO_{ads}, CO_{ads} and $CH_{3\,ads}$), and the fifth (OH_{ads}) to the secondary metal, according to the bimetallic catalyst assumption. Following previous work, there are two pathways leading to the production of adsorbed acetyl [20, 25, 54–56]: one through acetaldehyde production (Reactions 1 and 2) and other through the successive dehydrogenation of the carbon attached to the alcohol group (Reactions I and II). Ignoring the second pathway, as done by Meyer et al. [18], results in a reaction mechanism that is unable to predict product selectivities at low current densities [52]. For this reason, the second pathway is also considered in this work to enable the generation of acetic acid directly from ethanol even at low acetaldehyde production [16]. Following Meyer et al. [18], the two reaction pathways that emerge from adsorbed acetyl lead to the formation of either acetic acid (Reaction 4) or of CO_{ads} and $CH_{3\,ads}$ through the C–C bond breaking step (Reaction 5).

In the proposed kinetic mechanism, Reaction I represents the adsorption of ethanol to CH_3CHOH_{ads}. The net ethanol adsorption rate is given by the Butler-Volmer equation

$$q_{\mathrm{I}} = (1 - \Theta_{CH_3CHOH_{ads}} - \Theta_{CH_3CO_{ads}} - \Theta_{CO_{ads}} - \Theta_{CH_{3\,ads}})\, C_{\mathrm{E,acl}} k_{\mathrm{If}} \exp\left(\frac{\alpha_{\mathrm{I}} F}{RT}\eta_a\right)$$

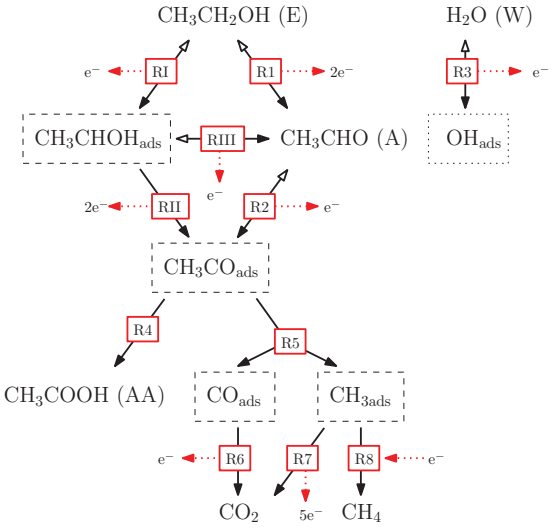

Figure 2: Reaction mechanism for the ethanol oxidation reaction (EOR) on binary Pt-based catalysts proposed in this work. Pt-site adsorbed species are indicated by a dashed box; OH_{ads} is boxed using dotted lines to indicate that it is adsorbed at the secondary metal sites. Reactions 4, 6 and 7 use the adsorbed hydroxyl groups to proceed. The exact stoichiometries are shown in Table 1.

$$- \Theta_{CH_3CHOH_{ads}} k_{Ib} \exp\left(-\frac{(1-\alpha_I)F}{RT}\eta_a\right) \quad (1)$$

where the factor between brackets in the forward reaction rate, which accounts for the blocking of active Pt-sites, does not include the adsorbed OH groups because in binary catalysts they are preferably attached to the secondary metal.

Reaction II describes the oxidation of CH_3CHOH_{ads} to CH_3CO_{ads}, whose reaction rate is given by

$$q_{II} = \Theta_{CH_3CHOH_{ads}} k_{II} \exp\left(\frac{\alpha_{II} 2F}{RT}\eta_a\right) \quad (2)$$

Note that this reaction is considered to occur in a single step, as possible intermediates are assumed to produce no other species [20, 24, 25]. Like other reactions between adsorbates, Reaction II is considered to be irreversible, hence the reaction rate given in Equation (2) accounts only for the forward reaction.

CH_3CHOH_{ads} can also be desorbed to give acetaldehyde through Reaction III. The net reaction rate is given by

$$q_{III} = \Theta_{CH_3CHOH_{ads}} k_{IIIf} \exp\left(\frac{\alpha_{III} F}{RT}\eta_a\right)$$
$$- (1 - \Theta_{CH_3CHOH_{ads}} - \Theta_{CH_3CO_{ads}} - \Theta_{CO_{ads}} - \Theta_{CH_3\,ads})$$
$$\times C_{A,acl} k_{IIIb} \exp\left(-\frac{(1-\alpha_{III})2F}{RT}\eta_a\right) \quad (3)$$

Table 1: The 11-step reaction mechanism proposed in this work.

Reaction			n_α
I. $CH_3CH_2OH \rightleftharpoons CH_3CHOH_{ads} + H^+ + e^-$	k_{If}	α_I	1
	k_{Ib}		1
II. $CH_3CHOH_{ads} \rightarrow CH_3CO_{ads} + 2H^+ + 2e^-$	k_{IIf}	α_{II}	2
	k_{IIb}		2
III. $CH_3CHOH_{ads} \rightleftharpoons CH_3CHO + H^+ + e^-$	k_{IIIf}	α_{III}	1
	k_{IIIb}		1
1. $CH_3CH_2OH \rightleftharpoons CH_3CHO + 2H^+ + 2e^-$	k_{1f}	α_1	2
	k_{1b}		2
2. $CH_3CHO \rightleftharpoons CH_3CO_{ads} + H^+ + e^-$	k_{2f}	α_2	1
	k_{2b}		1
3. $H_2O \rightleftharpoons OH_{ads} + H^+ + e^-$	k_{3f}	α_3	1
	k_{3b}		1
4. $CH_3CO_{ads} + OH_{ads} \longrightarrow CH_3COOH$	k_4		
5. $CH_3CO_{ads} \longrightarrow CO_{ads} + CH_{3\,ads}$	k_5		
6. $CO_{ads} + OH_{ads} \longrightarrow CO_2 + H^+ + e^-$	k_6	α_6	1
7. $CH_{3\,ads} + 2OH_{ads} \longrightarrow CO_2 + 5H^+ + 5e^-$	k_7	α_7	5
8. $CH_{3\,ads} + H^+ + e^- \longrightarrow CH_4$	k_8	α_8	1

In our extended reaction model, Reaction III is considered to be reversible, with acetaldehyde being also produced from ethanol by Reaction 1 and oxidized to CH_3CO_{ads} through Reaction 2 [20, 24, 25]. In this case, the backward reaction rate is proportional to the concentration of acetaldehyde and to the available Pt-sites.

Reaction 1 represents the redox reaction between ethanol and acetaldehyde. Under the bimetallic catalyst assumption, the net reaction rate is given by

$$q_1 = (1 - \Theta_{CH_3CHOH_{ads}} - \Theta_{CH_3CO_{ads}} - \Theta_{CO_{ads}} - \Theta_{CH_{3\,ads}}) \times \left[C_{E,acl} k_{1f} \exp\left(\frac{\alpha_1 2F}{RT}\eta_a\right) - C_{A,acl} k_{1b} \exp\left(-\frac{(1-\alpha_1)2F}{RT}\eta_a\right)\right] \quad (4)$$

As discussed above, the oxidation of acetaldehyde to CH_3CO_{ads} is described by Reaction 2, with the net reaction rate given by

$$q_2 = (1 - \Theta_{CH_3CO_{ads}} - \Theta_{CO_{ads}} - \Theta_{CH_3\,ads})\, C_{A,acl} k_{2f} \exp\left(\frac{\alpha_2 F}{RT}\eta_a\right) - \Theta_{CH_3CO_{ads}} k_{2b} \exp\left(-\frac{(1-\alpha_2)F}{RT}\eta_a\right) \quad (5)$$

The dissociative adsorption of water to yield adsorbed hydroxyl groups is represented by Reaction 3. The water activation rate, which in binary Pt-based catalysts occurs on the secondary metal, is given by

$$q_3 = k_{3f}\,(1 - \Theta_{OH_{ads}}) \exp\left(\frac{\alpha_3 F}{RT}\eta_a\right) - k_{3b}\Theta_{OH_{ads}} \exp\left(-\frac{(1-\alpha_3)F}{RT}\eta_a\right) \quad (6)$$

Reaction 4 describes the formation of acetic acid from adsorbed acetyl and hydroxyl groups. Since this reaction does not involve charge transfer it is independent of the anode overpotential, and its rate can be written as

$$q_4 = k_4 \Theta_{CH_3CO_{ads}} \Theta_{OH_{ads}} \quad (7)$$

An alternative pathway for the subsequent oxidation of acetyl starts with the breaking of the C–C bond to give CO_{ads} and CH_{3ads}. The rate of the C–C bond breaking step, represented by Reaction 5, does not involve charge transfer either, so it is simply proportional to the acetyl coverage factor

$$q_5 = k_5 \Theta_{CH_3CO_{ads}} \quad (8)$$

The CO_{ads} produced in Reaction 5 can be further oxidized to CO_2 using an adsorbed hydroxyl group following Reaction 6. The corresponding rate of CO_2 production from CO_{ads} is given by

$$q_6 = k_6 \Theta_{CO_{ads}} \Theta_{OH_{ads}} \exp\left(\frac{\alpha_6 F}{RT}\eta_a\right) \quad (9)$$

Although the final fate of the adsorbed CH_3-fragment is not clear, Meyer et al. [18] presumed that it was either oxidized to CO_2 with the help of two OH-groups through Reaction 7, or reduced at low potentials to CH_4 following Reaction 8. The corresponding rates of CH_{3ads} oxidation and reduction to carbon dioxide and methane are respectively given by

$$q_7 = k_7 \Theta_{CH_3\,ads} \Theta_{OH_{ads}}^2 \exp\left(\frac{\alpha_7 5 F}{RT}\eta_a\right) \quad (10)$$

and

$$q_8 = k_8 \Theta_{CH_3\,ads} \exp\left(-\frac{\alpha_8 F}{RT}\eta_a\right) \quad (11)$$

To determine the coverage factors of the five adsorbed species (CH_3CHOH_{ads}, CH_3CO_{ads}, CO_{ads}, $CH_{3\,ads}$, and OH_{ads}) the steady-state approximation (SSA) is applied to all of them, which yields the following set of equations

$$CH_3CHOH_{ads}: \quad q_{\mathrm{I}} - q_{\mathrm{II}} - q_{\mathrm{III}} = 0 \tag{12}$$

$$CH_3CO_{ads}: \quad q_2 + q_{\mathrm{II}} - q_5 - q_4 = 0 \tag{13}$$

$$OH_{ads}: \quad q_3 - q_4 - q_6 - 2q_7 = 0 \tag{14}$$

$$CO_{ads}: \quad q_5 - q_6 = 0 \tag{15}$$

$$CH_{3\,ads}: \quad q_5 - q_8 - q_7 = 0 \tag{16}$$

As shown in the Appendix, upon substitution of expressions (1)–(11) for the net reaction rates q_r into Eqs. (12)–(16), a system of five non-linear algebraic equations is obtained for the five coverage factors Θ_k. After some algebraic manipulations, the system can be reduced to a fifth-order polynomial equation for $\Theta_{OH_{ads}}$, which can be shown to have a real root between 0 and 1. This root can be obtained numerically for specified values of the ethanol and acetaldehyde concentrations at the anode catalyst layer, $C_{\mathrm{E,acl}}$ and $C_{\mathrm{A,acl}}$, and of the anode overpotential, η_a, readily yielding the remaining coverage factors from algebraic expressions. The cell temperature, T, and the set of kinetic parameters (including the rate constants, k_k, and transfer coefficients, α_k) must also be specified, and will be kept constant throughout the iterative solution process.

It is worth noting that, unlike previous models [18, 52], here the coverage factors depends explicitly on the concentration of ethanol at the anode catalyst layer, $C_{\mathrm{E,acl}}$, through the net reaction rate q_{I}. The reason is that our reaction mechanism includes, as previously stated, the production of CH_3CHOH_{ads} through Reaction I as a possible pathway for the oxidation of ethanol to CH_3CO_{ads}, which has not been explicitly considered in previous studies.

Once the coverage factors are known, the area specific net production (or consumption) rates of the free species, expressed in moles produced (or consumed) per unit time and per unit surface area of anode catalyst layer, can be written as

$$\omega_{\mathrm{E}} = -(q_{\mathrm{I}} + q_1)\,\delta_{\mathrm{acl}} \tag{17}$$

$$\omega_{\mathrm{A}} = (q_1 + q_{\mathrm{III}} - q_2)\,\delta_{\mathrm{acl}} \tag{18}$$

$$\omega_{\mathrm{AA}} = q_4 \delta_{\mathrm{acl}} \tag{19}$$

$$\omega_{CO_2} = (q_6 + q_7)\,\delta_{\mathrm{acl}} \tag{20}$$

$$\omega_{CH_4} = q_8 \delta_{\mathrm{acl}} \tag{21}$$

$$\omega_{\mathrm{W}} \quad = -q_3 \delta_{\mathrm{acl}} \tag{22}$$

where the subscript W denotes water. With this notation, positive (or negative) values of ω_k indicate net production (or consumption) of species k. Multiplying the area specific reaction rates, $q_r \delta_{\mathrm{acl}}$, by the number of electrons transferred in each reaction, n_r, adding the resulting electron generation rates all together and multiplying by Faraday's constant provides the current density generated at the anode catalyst layer

$$i = F\left(q_{\mathrm{I}} + 2q_{\mathrm{II}} + q_{\mathrm{III}} + 2q_1 + q_2 + q_3 + q_6 + 5q_7 - q_8\right)\delta_{\mathrm{acl}} \tag{23}$$

Note in particular the relevant role of Reaction 7, which releases 5 electrons and therefore may have a significant impact on the total current density generation even for moderately low values of q_7.

3.2. Anode gas diffusion layer (agdl).

The net molar flux of the free reacting species, transported by convection and diffusion from the bulk fluid in the anode channel (ac) to the anode channel/gas diffusion layer interface (agdl/ac), is modeled using an overall mass transport coefficient h [40, 46], which allows to write

$$N_k = -h\left(C_{k,\mathrm{ac}} - C_{k,\mathrm{ac/agdl}}\right) \qquad k = \mathrm{E}, \mathrm{A} \tag{24}$$

where $C_{k,\mathrm{ac}}$ represents the bulk concentration of species k in the anode channel, and $C_{k,\mathrm{ac/agdl}}$ is the concentration of species k at the ac/agdl interface. Note that the sign of N_k indicates whether the net molar flux of species k is directed in the positive or negative y-direction, with $N_k > 0$ indicating that the net molar flux of species k goes from the catalyst layer to the flow channel, while for $N_k < 0$ it goes from the channel to the catalyst layer.

The mass transport of free species across the gas diffusion layer is driven by Fickian diffusion and by the convective drag of water flowing through the gas diffusion layer

$$N_k = -D^{\mathrm{eff}}_{k,\mathrm{agdl}} \frac{\partial C_k}{\partial y} + v_{\mathrm{W}} C_k \qquad k = \mathrm{E}, \mathrm{A} \tag{25}$$

where $D^{\mathrm{eff}}_{k,\mathrm{agdl}} = \epsilon^{3/2} D_{k,\mathrm{W}}$ is the effective diffusivity of species k in the porous media, expressed using Bruggeman correction in terms of the porosity ϵ of the gas diffusion layer and of the bulk diffusivity $D_{k,\mathrm{W}}$ of species k in water. Although this correction is known to overestimate the effective diffusivity [57, 58], it is also the most extended assumption for the description of diffusive transport in DEFC [18, 40, 48, 51] and therefore will be adopted here for simplicity. The values of the bulk diffusivity and gdl porosity used in this work are shown in Table 4.

A more realistic description of diffusive transport in the gas diffusion layer would have required accounting for two-dimensional effects coming from the rib-channel pattern, including, e.g., porosity variations [59] across the porous layer, or the use of a 3.5 exponent for the through-plane effective diffusivity [57]. However, the lack of agreement in the values of the diffusion coefficients reported in the literature, with values from 1/3 [18] to 3 [10, 40, 43] times the one considered here, makes it meaningless to consider a more complex model. Moreover, the role of mass transport in the current density range where the reaction mechanism will be fitted to experimental results is anticipated to be unimportant because those currents are moderately far from the limiting current density.

Equation (25) involves the average velocity of water across the gas diffusion layer

$$v_{\mathrm{W}} = \frac{W_{\mathrm{W}}}{\rho_{\mathrm{W}}}\left(\omega_{\mathrm{W}} - n_d^{\mathrm{W}}\frac{i}{F}\right) \tag{26}$$

which is induced by the water consumption rate ω_{W} (< 0) at the anodic reaction and the electro-osmotic flux of water crossing the membrane, to be addressed below. Note that with the transverse y-coordinate pointing from cathode to anode (see Figure 1), the water velocity v_w must be negative, since water always moves from anode to cathode.

Integrating Equation (25) across the gas diffusion layer, with boundary conditions $C_k = C_{k,\mathrm{ac/agdl}}$ at the ac/agdl interface and $C_k = C_{k,\mathrm{acl}}$ at the acl, and making use of (24) to eliminate $C_{k,\mathrm{ac/agdl}}$ from the resulting expression, the molar flux of species k can be written as [41]

$$N_k\left(C_{k,\mathrm{ac}}; C_{\mathrm{E,acl}}, C_{\mathrm{A,acl}}, \eta_a\right) = -\frac{C_{k,\mathrm{ac}}e^{v_{\mathrm{W}}/k_{k,\mathrm{gdl}}} - C_{k,\mathrm{acl}}}{e^{v_{\mathrm{W}}/k_{k,\mathrm{gdl}}}\left(1 + v_{\mathrm{W}}/h\right) - 1}\, v_{\mathrm{W}} \qquad k = \mathrm{E, A} \tag{27}$$

where $k_{k,\mathrm{agdl}} = D^{\mathrm{eff}}_{k,\mathrm{agdl}}/\delta_{\mathrm{acl}}$ denotes the diffusive mass transfer coefficient of the gas diffusion layer.

It should be noted that the molar fluxes given in Equation (27) are a function of $C_{\mathrm{E,acl}}$, $C_{\mathrm{A,acl}}$, and η_a, because the water velocity v_{W} given in (26) depends both on ω_{W} and i, which in turn depend on $C_{\mathrm{E,acl}}$, $C_{\mathrm{A,acl}}$, and η_a. As will be shown below, the values of $C_{\mathrm{E,acl}}$ and $C_{\mathrm{A,acl}}$ must be determined iteratively from the solution of the full mass transport problem, which includes the effect of ethanol and acetaldehyde crossover.

3.3. Ethanol and acetaldehyde crossover.

The permeation of ethanol and other reactive species, such as acetaldehyde, through the polymeric membrane constitutes a severe problem in DEFCs. The reactive species that cross the membrane are prone to react electrochemically with oxygen at the cathode catalyst, which results in a parasitic current that increases the cathode overpotential. But this is not the only effect of crossover, which is also

noticeable at the anode electrode, where a fraction of the fuel that reaches the active region of the cell leaks across the membrane due to the crossover flux. This reduces the amount of fuel that is available to produce current at the anode catalyst layer, thereby increasing the so-called concentration overpotential.

The hypothesis that the membrane is impermeable to gases implies that oxygen crossover should be ignored. Jablonski et al. [22] detected the presence of acetaldehyde and acetic acid in the anode outlet stream under open circuit conditions, which was attributed to the parasitic electro-oxidation of ethanol at the anode electrode with the oxygen crossing the membrane from cathode to anode. Their experiments were carried out with pure oxygen feed at 200 kPa cathode pressure, which could have accentuated the oxygen crossover rate. This effect, however, is anticipated to be less important for fuel cells operated with air at nearly atmospheric pressure. By way of contrast, James and Pickup [38] attributed the presence of acetaldehyde and acetic acid in the anode outlet to the parasitic electrooxidation of ethanol at the cathode side followed by the back diffusion of those two products to the anode side, from where they were evacuated by the anode liquid stream. The lack of agreement found in the literature and the small quantitative effect of oxygen crossover justify, in any case, ignoring the crossover of oxygen in the analysis.

As a result, in our model we shall consider only the effect of ethanol an acetaldehyde crossover, since in low-temperature DEFCs they are the only reacting free species that generate electrons in the EOR. Just like the crossover flux of methanol in DMFCs [53], the crossover flux of ethanol and acetaldehyde are driven by Fickian diffusion and electro-osmotic drag

$$N_{k,\mathrm{cross}}\left(C_{\mathrm{E,acl}}, C_{\mathrm{A,acl}}, \eta_a\right) = -D^{\mathrm{eff}}_{k,\mathrm{mem}} \frac{\partial C_{k,\mathrm{acl}}}{\partial y} + n_d^k \frac{i}{F} \qquad k = \mathrm{E, A} \quad (28)$$

where $D^{\mathrm{eff}}_{k,\mathrm{mem}}$ is the effective diffusivity of species k in the membrane and n_d^k is the electro-osmotic drag coefficient of species k, defined as the number of molecules of species k dragged by a proton crossing the membrane. For low species concentrations, this coefficient can be expressed in terms of the electro-osmotic drag coefficient of water, n_d^{W}, as

$$n_d^k = \frac{W_{\mathrm{W}}}{\rho_{\mathrm{W}}} n_d^{\mathrm{W}} C_{k,\mathrm{acl}} \quad (29)$$

where W_{W} is the molecular weight of water, ρ_{W} is the density of water, and n_d^{W} is given in terms of temperature by [60]

$$n_d^w = 2.9 \exp\left[1029\left(\frac{1}{333} - \frac{1}{T}\right)\right] \quad (30)$$

Assuming that the electro-oxidation of both ethanol and acetaldehyde in the cathode electrode is fast enough for the resulting concentrations of both species at the cathode catalyst layer to be much smaller than those at the anode catalyst layer, the crossover fluxes can be written in first approximation as

$$N_{k,\mathrm{cross}}\left(C_{\mathrm{E,acl}}, C_{\mathrm{A,acl}}, \eta_a\right) = -\left[\frac{D^{\mathrm{eff}}_{k,\mathrm{mem}}}{\delta_{\mathrm{mem}}} + \frac{W_{\mathrm{W}}}{\rho_w} n_d^{\mathrm{W}} \frac{i}{F}\right] C_{k,\mathrm{acl}} \qquad k = \mathrm{E, A} \quad (31)$$

3.4. Determination of the free species concentrations.

The concentrations of ethanol and acetaldehyde at the anode catalyst layer are determined from the local mass balance of ethanol and acetaldehyde at this layer. Imposing that the molar flux of ethanol (acetaldehyde) that reaches the acl by convection and diffusion from the anode backing must be equal to the rate of ethanol (acetaldehyde) consumption at the anode catalyst layer, plus the flux of ethanol (acetaldehyde) that crosses the membrane, yields the two equations

$$N_{\mathrm{E}}\left(C_{\mathrm{E,ac}}; C_{\mathrm{E,acl}}, C_{\mathrm{A,acl}}, \eta_a\right) = \omega_{\mathrm{E}}\left(C_{\mathrm{E,acl}}, C_{\mathrm{A,acl}}, \eta_a\right) - N_{\mathrm{E,cross}}\left(C_{\mathrm{E,acl}}, C_{\mathrm{A,acl}}, \eta_a\right) \quad (32)$$

$$N_{\mathrm{A}}\left(C_{\mathrm{A,ac}}; C_{\mathrm{E,acl}}, C_{\mathrm{A,acl}}, \eta_a\right) = \omega_{\mathrm{A}}\left(C_{\mathrm{E,acl}}, C_{\mathrm{A,acl}}, \eta_a\right) - N_{\mathrm{A,cross}}\left(C_{\mathrm{E,acl}}, C_{\mathrm{A,acl}}, \eta_a\right) \quad (33)$$

where the molar fluxes N_k reaching the acl are given by (27), the electrochemical consumption rates ω_k by (17) and (18), and the crossover fluxes $N_{k,\mathrm{cross}}$ by (31). Note that Eqs. (32) and (33) do not show the explicit dependence of the different terms on the cell temperature T and the reaction constants, which are assumed to remain unchanged during the iterative solution process.

Given the channel concentrations, $C_{\mathrm{E,ac}}$ and $C_{\mathrm{A,ac}}$, and the anode overpotential, η_a, equations (32) and (33) represent a system of two non-linear algebraic equations for the two unknowns $C_{\mathrm{E,acl}}$ and $C_{\mathrm{A,acl}}$ that must be solved numerically. To this end, we used the *fsolve* routine from the MATLAB optimization toolbox, specifying sufficiently small values for the concentrations of ethanol and acetaldehyde (e.g., $C^0_{\mathrm{E,acl}} = C^0_{\mathrm{E,acl}} = 0.05$ M) as suitable initial guesses to avoid reaching negative spurious solutions during the iterative process. The concentration of the remaining non-adsorbed species (i.e., acetic acid, CO_2, and CH_4) at the acl, which do not influence the electro-oxidation rate of ethanol and acetaldehyde, could be obtained *a posteriori* from the corresponding mass balances.

3.5. Product selectivity.

As widely seen in the literature, a handy index to analyze the product distribution in DEFCs is the product selectivity [16, 19, 61], defined as the fractional amount of the overall molar production rate corresponding to a given species k. In DEFCs, the product selectivity of species k can be calculated as follows

$$s_k\ [\%] = \frac{\omega_k}{\omega_{\mathrm{A}} + \omega_{\mathrm{AA}} + \omega_{\mathrm{CO_2}} + \omega_{\mathrm{CH_4}}} \qquad k = \mathrm{E, A, CO_2, CH_4} \tag{34}$$

in terms of the molar production rates of the different products generated by the EOR. The product selectivities can also be expressed in terms of the net reaction rates q_r as follows

$$\begin{aligned} s_{\mathrm{A}} &= \frac{q_1 + q_{\mathrm{III}} - q_2}{q_1 + q_{\mathrm{III}} - q_2 + q_4 + q_6 + q_7 + q_8} \\ s_{\mathrm{AA}} &= \frac{q_4}{q_1 + q_{\mathrm{III}} - q_2 + q_4 + q_6 + q_7 + q_8} \\ s_{\mathrm{CH_4}} &= \frac{q_8}{q_1 + q_{\mathrm{III}} - q_2 + q_4 + q_6 + q_7 + q_8} \\ s_{\mathrm{CO_2}} &= \frac{q_6 + q_7}{q_1 + q_{\mathrm{III}} - q_2 + q_4 + q_6 + q_7 + q_8} \end{aligned} \tag{35}$$

expressions obtained by substituting the ω_k given in (17)–(22) into Equation (34).

3.6. Model fitting procedure.

A simulation campaign was carried out to validate the model predictions against experimental data reported in the literature. The comparison was limited to the polarization curve of the anode electrode, and to the selectivity index s_k of the main products, k = acetaldehyde (A), acetic acid (AA), carbon dioxide (CO_2), and methane (CH_4). As part of the model set-up process, a set of reaction constants was calculated to fit the model to the available experimental results of selectivity and anode overpotential [16], the latter obtained with the aid of a dynamic hydrogen electrode. An optimization procedure was used to obtain the set of reaction constants. As in previous work [52], the built-in *gamultiobj* multiobjective genetic algorithm solver, available in MATLAB, was used to optimize an objective function. The objective function used was the quadratic norm of the relative errors for the current density, acetaldehyde, acetic acid, an CO_2 selectivities for the pair of anode overpotentials 0.3375 V and 0.4009 V

$$\mathrm{err} = \sqrt{\sum_i \left(\frac{x_{i,\mathrm{LP}} - x_i}{x_{i,\mathrm{LP}}} \right)^2} \tag{36}$$

where $x_{i,\mathrm{LP}}$ denote the current density and product selectivities reported by Li & Pickup [16], which are summarized in Table 2, and x_i is the corresponding value computed with the present model. The set of

reaction constants and transfer coefficients obtained in [52] was used as initial population for Reactions 1 to 8. For Reactions I to III the initial population was obtained adopting the reaction constants of similar reactions found in the original mechanism of Meyer et al. [18]. For instance, Reactions I and III are adsorption/desorption reactions, just like Reaction 2; whereas Reaction II is a reaction between adsorbed species, just like Reaction 5. The set of reaction constants and transfer coefficients obtained from the optimization process is shown in Table 3. The reaction constants and transfer coefficients reported in previous works are also included for comparative purposes.

Table 2: Experimentally measured product selectivity data reported by Li & Pickup [16].

η_a [V]	0.3375	0.4009
i [A m^{-2}]	300	600
s_{A}	0.165	0.377
s_{AA}	0.768	0.556
$s_{\mathrm{CO_2}}$	0.067	0.067

3.7. Effective electron generation number.

Each ethanol molecule consumed in the EOR may follow one of the three main chemical paths represented in Figure 2: acetaldehyde production, acetic acid production or C–C bond breaking. The first path produces one molecule of acetaldehyde for each molecule of ethanol consumed and releases 2 electrons. The second path produces one molecule of acetic acid for each molecule of ethanol, releasing 4 electrons instead. The third path proceeds through the C–C bond breaking step, and therefore produces two single carbon molecules for each molecule of ethanol consumed. These two molecules may be either a CO_2 and a CH_4 molecule (produced by Reactions 6 and 8 releasing 4 electrons) or two CO_2 molecules (produced by Reactions 6 and 7 releasing 12 electrons) depending on the final fate of the adsorbed methyl group. While the carbonyl group is always oxidized to CO_2 through Reaction 6, the methyl group can be either oxidized to CO_2 through Reaction 7 or reduced to CH_4 through reaction 8. As a result, the generation of a CO_2 molecule by Reaction 6 is always accompanied either by the production of another CO_2 molecule by Reaction 7 or by the production of a CH_4 molecule by Reaction 8. As a result, the molar production rate of CO_2 by Reaction 6 must be equal to the sum of the molar production rates of CO_2 and CH_4 by Reactions 7 and 8

$$q_6 = q_7 + q_8 \tag{37}$$

Table 3: Sets of reactions constants and charge transfer coefficients originally reported by Meyer et al. [18], and genetically optimized to fit Li & Pickup's [16] overpotential and product selectivity data using Meyer et al.'s mechanism and the extended mechanism proposed in this work.

Constant	Meyer et al. [18]	Meyer et al. [18] fitted to [16]	Extended mechanism fitted to [16]
k_{If} $\left[\mathrm{s}^{-1}\right]$	–	–	0.3306
k_{Ib} $\left[\mathrm{mol\ m^{-3}\ s^{-1}}\right]$	–	–	1.8×10^{-3}
k_{II} $\left[\mathrm{mol\ m^{-3}\ s^{-1}}\right]$	–	–	1.34×10^{2}
k_{IIIf} $\left[\mathrm{mol\ m^{-3}\ s^{-1}}\right]$	–	–	1.01×10^{3}
k_{IIIb} $\left[\mathrm{s}^{-1}\right]$	–	–	22.67
$k_{1\mathrm{f}}$ $\left[\mathrm{s}^{-1}\right]$	2.8×10^{-6}	1.5×10^{-5}	3.49×10^{-5}
$k_{1\mathrm{b}}$ $\left[\mathrm{s}^{-1}\right]$	2.21×10^{-2}	1.86×10^{-2}	13.784
$k_{2\mathrm{f}}$ $\left[\mathrm{s}^{-1}\right]$	6.22×10^{-5}	8.92×10^{-4}	6.4×10^{-2}
$k_{2\mathrm{b}}$ $\left[\mathrm{mol\ m^{-3}\ s^{-1}}\right]$	10^{-8}	5.54×10^{-9}	10^{-4}
$k_{3\mathrm{f}}$ $\left[\mathrm{mol\ m^{-3}\ s^{-1}}\right]$	7.4×10^{-3}	3.5×10^{-3}	0.9619
$k_{3\mathrm{b}}$ $\left[\mathrm{mol\ m^{-3}\ s^{-1}}\right]$	1.8×10^{3}	1.8×10^{3}	1.01×10^{2}
k_4 $\left[\mathrm{mol\ m^{-3}\ s^{-1}}\right]$	2×10^{4}	3.4×10^{6}	2.77×10^{2}
k_5 $\left[\mathrm{mol\ m^{-3}\ s^{-1}}\right]$	10^{-7}	3.15×10^{4}	5.67
k_6 $\left[\mathrm{mol\ m^{-3}\ s^{-1}}\right]$	1.15×10^{-2}	9.53×10^{-1}	0.1391
k_7 $\left[\mathrm{mol\ m^{-3}\ s^{-1}}\right]$	10^{-14}	6.78×10^{9}	9.2
k_8 $\left[\mathrm{mol\ m^{-3}\ s^{-1}}\right]$	2.9×10^{-4}	7.42×10^{-4}	45.04
α_{I}	–	–	0.325
α_{II}	–	–	0.473
α_{III}	–	–	0.362
α_1	0.5	0.495	0.499
α_2	0.5	0.329	0.359
α_3	0.5	0.346	0.355
α_6	0.5	0.38	0.319
α_7	0.5	0.488	0.427
α_8	0.5	0.447	0.423

a result that follows mathematically from Eqs. (15) and (16).

To investigate the origin of the different species produced by the EOR, and in particular the chemical pathways leading to CO_2 formation, let us consider the following set of global reactions

$$CH_3CH_2OH \rightarrow CH_3CHO + 2H^+ + 2e^- \quad \text{(GR1)}$$

$$CH_3CH_2OH + H_2O \rightarrow CH_3COOH + 4H^+ + 4e^- \quad \text{(GR2)}$$

$$CH_3CH_2OH + H_2O \rightarrow CO_2 + CH_4 + 4H^+ + 4e^- \quad \text{(GR3)}$$

$$CH_3CH_2OH + 3H_2O \rightarrow 2CO_2 + 12H^+ + 12e^- \quad \text{(GR4)}$$

which represent, respectively, the overall processes leading to the generation of (GR1) acetaldehyde, (GR2) acetic acid, (GR3) CO_2 and CH_4 through Reactions 6 and 8, and (GR4) $2CO_2$ through Reactions 6 and 7, indicating the number of electrons released in each case. Hereafter the fraction of ethanol consumed by the different global reactions shall be denoted as the path selectivity, $s^{\mathrm{GR}j}$, $j = 1, 2, 3, 4$, such that $\sum_{j=1}^{4} s^{\mathrm{GR}j} = 1$. It is also convenient to introduce the effective electron generation number, n^{eff}, defined as the average number of electrons produced by each ethanol molecule consumed at the anode catalyst layer. This number, which gives us an idea about the overall effectiveness of the EOR in terms of current production, can be calculated from the path selectivities as

$$n^{\mathrm{eff}} = 2s^{\mathrm{GR1}} + 4s^{\mathrm{GR2}} + 4s^{\mathrm{GR3}} + 12s^{\mathrm{GR4}} \quad (38)$$

Note that this expression distinguishes the fractions of CO_2 produced by Reaction 6 that correspond either to (GR3) or (GR4).

The path selectivity of the four global reactions can be computed from the model results as

$$\begin{aligned} s^{\mathrm{GR1}} &= \frac{q_1 + q_{\mathrm{III}} - q_2}{|q_1 + q_{\mathrm{I}}|} \\ s^{\mathrm{GR2}} &= \frac{q_4}{|q_1 + q_{\mathrm{I}}|} \\ s^{\mathrm{GR3}} &= \frac{q_8}{|q_1 + q_{\mathrm{I}}|} \\ s^{\mathrm{GR4}} &= \frac{q_7}{|q_1 + q_{\mathrm{I}}|} \end{aligned} \quad (39)$$

where the denominator $|q_1 + q_{\mathrm{I}}|$ represents the ethanol consumption rate. The numerator of each path selectivity represents the rate of each global reaction according to the present model. Unlike the product selectivity, the path selectivity accounts for the fraction of ethanol that is consumed through each global reaction. A relationship between path and product selectivities is thus needed if we want to calculate the effective electron generation number from (38) using experimental data, which only provide product

selectivities. To this end, the product selectivities are first expressed in terms of the path selectivities as

$$\begin{aligned} s_{\mathrm{A}} &= \frac{s^{\mathrm{GR1}}}{s^{\mathrm{GR1}} + s^{\mathrm{GR2}} + 2\left(s^{\mathrm{GR3}} + s^{\mathrm{GR4}}\right)} \\ s_{\mathrm{AA}} &= \frac{s^{\mathrm{GR2}}}{s^{\mathrm{GR1}} + s^{\mathrm{GR2}} + 2\left(s^{\mathrm{GR3}} + s^{\mathrm{GR4}}\right)} \\ s_{\mathrm{CH_4}} &= \frac{s^{\mathrm{GR3}}}{s^{\mathrm{GR1}} + s^{\mathrm{GR2}} + 2\left(s^{\mathrm{GR3}} + s^{\mathrm{GR4}}\right)} \\ s_{\mathrm{CO_2}} &= \frac{s^{\mathrm{GR3}} + 2s^{\mathrm{GR4}}}{s^{\mathrm{GR1}} + s^{\mathrm{GR2}} + 2\left(s^{\mathrm{GR3}} + s^{\mathrm{GR4}}\right)} \end{aligned} \tag{40}$$

where it has been taken into account that, according to their global stoichiometries, (GR3) and (GR4) yield two molecules of reaction products for each molecule of ethanol consumed. The above expressions are not linearly independent because the sum of the product selectivities is equal to unity by definition. Using three of them together with the linear relation $\sum_{j=1}^{4} s^{\mathrm{GR}j} = 1$, one obtains a system of four linear equations for the four path selectivities, which can be readily inverted to give

$$\begin{aligned} s^{\mathrm{GR1}} &= \frac{s_{\mathrm{A}}}{s_{\mathrm{A}} + s_{\mathrm{AA}} + \frac{1}{2}\left(s_{\mathrm{CO_2}} + s_{\mathrm{CH_4}}\right)} \\ s^{\mathrm{GR2}} &= \frac{s_{\mathrm{AA}}}{s_{\mathrm{A}} + s_{\mathrm{AA}} + \frac{1}{2}\left(s_{\mathrm{CO_2}} + s_{\mathrm{CH_4}}\right)} \\ s^{\mathrm{GR3}} &= \frac{s_{\mathrm{CH_4}}}{s_{\mathrm{A}} + s_{\mathrm{AA}} + \frac{1}{2}\left(s_{\mathrm{CO_2}} + s_{\mathrm{CH_4}}\right)} \\ s^{\mathrm{GR4}} &= \frac{\frac{1}{2}\left(s_{\mathrm{CO_2}} - s_{\mathrm{CH_4}}\right)}{s_{\mathrm{A}} + s_{\mathrm{AA}} + \frac{1}{2}\left(s_{\mathrm{CO_2}} + s_{\mathrm{CH_4}}\right)} \end{aligned} \tag{41}$$

Using these expressions in Equation (38), the effective electron generation number can alternatively be written as

$$\begin{aligned} n^{\mathrm{eff}} &= \frac{2s_{\mathrm{A}} + 4s_{\mathrm{AA}} + 6s_{\mathrm{CO_2}} - 2s_{\mathrm{CH_4}}}{s_{\mathrm{A}} + s_{\mathrm{AA}} + \frac{1}{2}\left(s_{\mathrm{CO_2}} + s_{\mathrm{CH_4}}\right)} \\ &= \frac{2s_{\mathrm{A}} + 4s_{\mathrm{AA}} + 6s_{\mathrm{CO_2}} - 2s_{\mathrm{CH_4}}}{1 - \frac{1}{2}\left(s_{\mathrm{CO_2}} + s_{\mathrm{CH_4}}\right)} \end{aligned} \tag{42}$$

thereby enabling its evaluation either from experimental data or numerical/modeling results.

4. Results and discussion

All the results presented below were obtained using the fixed set of physical constants, mass transport properties and design parameters presented in Table 4. This includes, in particular, a constant ethanol feed concentration of 1 M, and a cell operating temperature of 70°C, values adopted from the available experimental data used to optimize the kinetic constants.

Table 4: Physical constants, mass transport coefficients and design parameters used in the 1D across-the-channel model.

Property	Value	Reference
Molecular diffusivity of ethanol in water, $D_{E,W}$	10^{-9} m^{2}s^{-1}	[62]
Molecular diffusivity of acetaldehyde in water, $D_{A,W}$	10^{-9} m^{2}s^{-1}	[62]
Molecular diffusivity of ethanol in membrane, $D_{E,mem}$	10^{-9} m^{2}s^{-1}	[40]
Molecular diffusivity of acetaldehyde in membrane, $D_{A,mem}$	10^{-9} m^{2}s^{-1}	[40]
GDL porosity, ϵ	0.78	[18]
Mass transfer coefficient ac/agdl, h	10^{-6} m s^{-1}	Assumed
Anode gdl thickness, δ_{agdl}	280 μm	[18]
Anode cl thickness, δ_{acl}	20 μm	[18]
Membrane thickness, δ_{mem}	178 μm	[18]
Ethanol feed concentration, $C_{E,ac}$	1 M	Assumed
Temperature, T	70°C	Assumed

Figure 3 shows the anode polarization curve predicted by the present model compared against the experimental data of Li & Pickup [16]. As can be seen, the model, optimized genetically to fit both the polarization and product selectivity data, correctly reproduces the anode overpotential in the whole current density range. For comparative purposes, the figure also shows the anode polarization curve reported by Meyer et al. [18]. When using the reaction mechanism and kinetic parameters suggested by Meyer et al. [18], the polarization curve predicted by our model also agrees well with the experimental data, although the range of power densities under study is significantly narrower in this case.

Figures 4a, 4b and 4c show the variation of the product selectivities with the current density predicted by the present model compared with the experimental data reported by Li & Pickup [16]. It is seen that acetaldehyde (A), acetic acid (AA), and CO_2 selectivities are correctly reproduced at both high and low currents. The experimental data used to optimize the kinetic parameters of Table 2 precludes the production of methane at the current densities under study. However, the model predicts a slight methane yield ($s_{CH_4} \sim 0.05$) at very low currents (< 3 mA/cm^2), although no experimental data is available to confirm this result. Summarizing, the experimental results show that acetaldehyde selectivity increases with current density, while acetic acid decreases and CO_2 remains unchanged. These trends are correctly predicted by the optimized kinetic model. However, when using the mechanism of Meyer et al. [18] the predicted selectivity of acetaldehyde remains above 90% up to 50 mA/cm^2, in contrast with the much

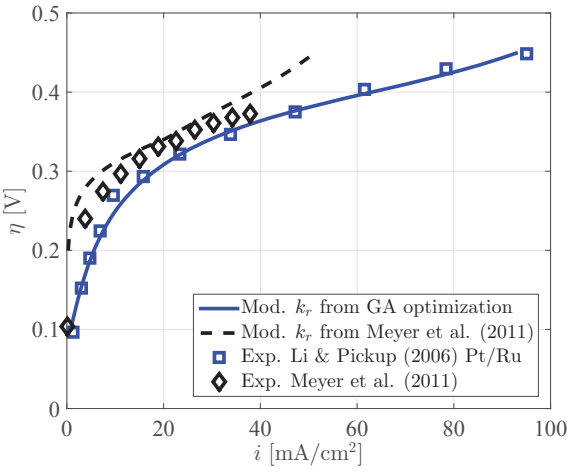

Figure 3: Anode overpotential measured experimentally by Meyer et al. [18] and Li & Pickup [16] and computed with the present model optimized to fit Li & Pickup's [16] overpotential and product selectivity data (solid line), and using the set of reaction constants proposed by Meyer et al. [18] (dashed line).

lower values measured by Li & Pickup [16] and captured by the new model. Interestingly enough, the new reaction mechanism yields much better agreement in terms of product selectivities also when the mechanism by Meyer et al. [18] is supplied with a genetically optimized set of reaction constants, as has been recently shown by the authors elsewhere [52].

The improved performance of the extended model, particularly in terms of product selectivity, stems from the fact that it is not biased towards the formation of acetaldehyde like the mechanism originally proposed by Meyer et al. [18], which hinders the production of acetic acid at low current densities due to the acetaldehyde bottleneck effect [52]. By contrast, the new model is able to predict high acetic acid selectivities at low currents thanks to the new chemical pathway involving adsorbed species (Reactions I, II and III). The improvement is also observed in the predicted effective electron generation number. As seen in Figure 4d, the new model predicts values of $n^{\text{eff}} \simeq 4$ for all current densities in agreement with the experimental data reported in [16, 61]. The agreement disappears when using the reaction mechanism of Meyer et al. [18], which result in values of $n^{\text{eff}} \simeq 2$ much lower than those observed experimentally.

As previously discussed, the proposed model exhibits two paths leading to the production of adsorbed acetyl: one through acetaldehyde production (Reactions 1 and 2) and other through CH_3CHOH_{ads} (Reactions I and II). The numerical results show that this dual path fits perfectly in the full current density range. Figures 5 and 6 show, respectively, the net reaction rate of all the elementary reactions involved in the new mechanism and the area specific molar production (A, AA ans CO_2) and consumption (E and W) rates of the free species. Ethanol is consumed by two reactions, Reactions 1 and I, with a net

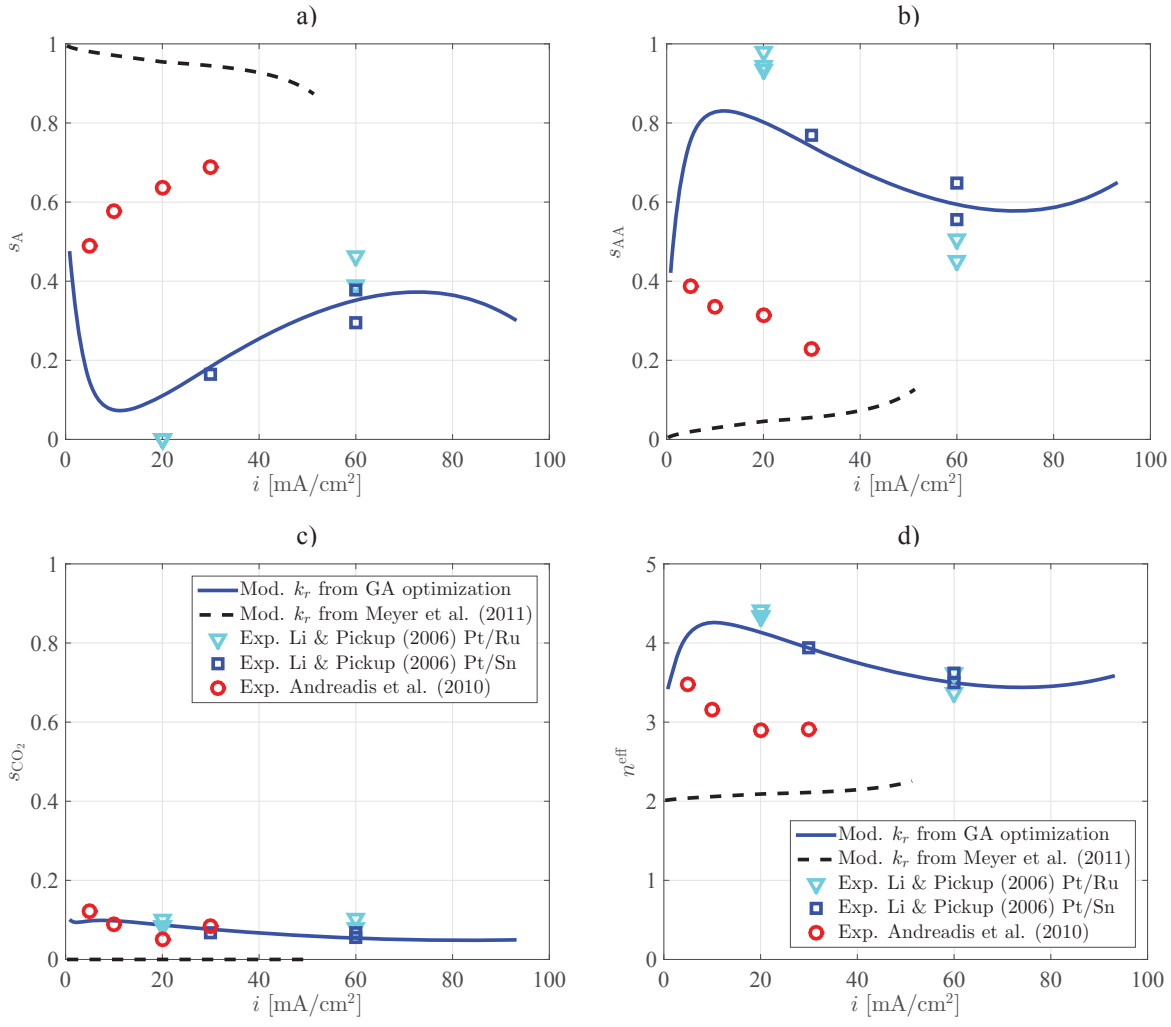

Figure 4: Variation of a) acetaldehyde, b) acetic acid, and c) CO_2 selectivity, and d) the effective electron generation number with the current density as obtained with the present model optimized to fit Li & Pickup's [16] overpotential and product selectivity data (solid line), and using the set of reaction constants proposed by Meyer et al. [18] (dashed line).

consumption rate given by Equation (17). At low currents ethanol consumption proceeds mainly through Reaction I, while at high currents Reaction 1 takes over and becomes dominant although Reaction I still contributes significantly.

Acetaldehyde is the only free intermediate species and therefore plays a crucial role in the EOR. It is produced by Reactions 1 and III and consumed by Reaction 2, with a net production rate given by Equation (18). As can be see, at low current densities acetaldehyde production occurs mainly through Reaction III. The rate of this reaction decreases steadily and is soon surpassed by that of Reaction 1, which constitutes the main path for acetaldehyde production at high currents. Acetaldehyde consumption becomes also significant at high currents, when the rate of Reaction 2 approaches that of Reaction 1. At

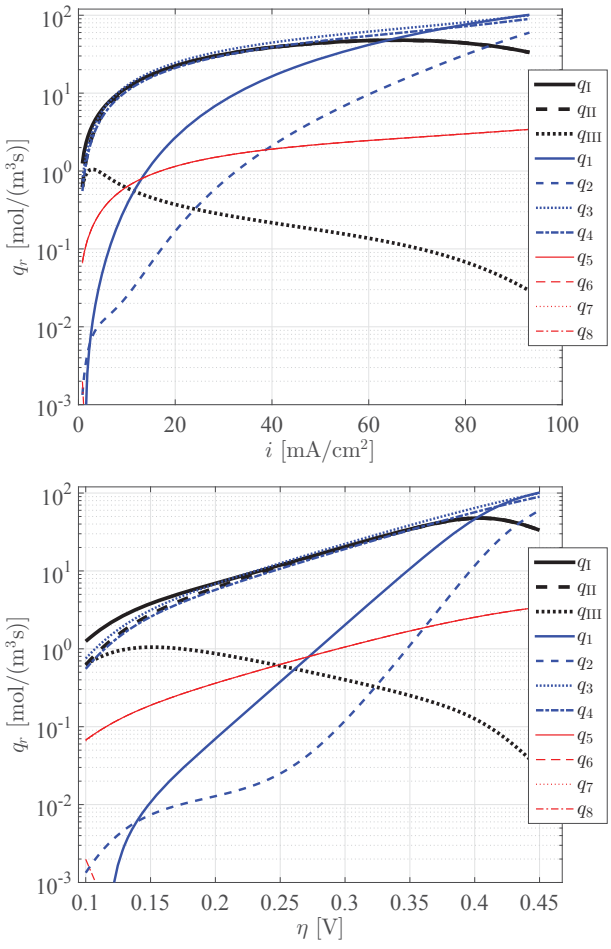

Figure 5: Net reaction rate of all the reactions involved in the model plotted as a function of current density (top) and anode overpotential (bottom). Calculation performed with the set of reactions constants optimized to fit Li & Pickup's [16] overpotential and product selectivity data. Note that since $q_5 = q_6 = q_7 + q_8$, with $q_8 \ll q_7$, the curves for q_5, q_6 and q_7 are indistinguishable.

this point, net acetaldehyde production starts to decline due to the effect of mass transport losses, since ethanol starvation forces the cell to draw current from acetaldehyde consumption. Note also that at low-to-medium currents the net production rate of acetaldehyde is relatively small compared to other species, particularly acetic acid, leading to the low acetaldehyde selectivity shown in Figure 4a in agreement with the experimental data reported in literature [16, 61]. By way of contrast, a significantly higher acetaldehyde selectivity is predicted at very low currents due to production through Reaction III, although no experimental data is available to validate this results.

Figure 7 shows the coverage factors of the five adsorbed species plotted as a function of the anode overpotential. The numerical results exhibit high CO_{ads} occupation at low-to-medium overpotentials,

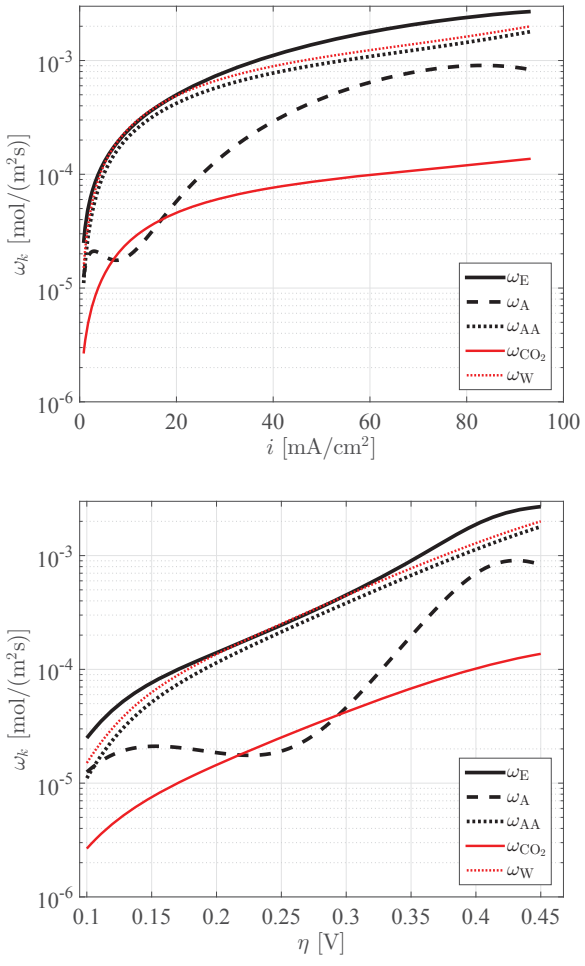

Figure 6: Net production and consumption rates of the five free species involved in the model plotted as a function of current density (top) and anode overpotential (bottom). Calculation performed with the set of reactions constants optimized to fit Li & Pickup's [16] overpotential and product selectivity data.

with representative values $\Theta_{CO_{ads}} = \{0.95, 0.9, 0.85, 0.8\}$ occurring for $\eta = \{0.167, 0.233, 0.273, 0.303\}$. At higher overpotentials, the Pt-sites left free by the carbonyl groups are occupied by adsorbed acetyl molecules, which promotes the production of acetic acid and the C–C bond breaking step. Figure 5 shows that the former (q_4) is significantly faster than the latter (q_5), with a ratio between both reaction rates of order 20 for all current densities. As a result, low CO_2 selectivity is observed at low and high overpotentials. Kavanagh el al. [25] attributed the low CO_2 selectivity at low overpotentials to the unavailability of oxidants, which inhibits the electro-oxidation of CO_{ads} to CO_2, the former effectively acting as a poisoning species. This is compatible with the high CO_{ads} occupation observed in Figure 7 at low-to-medium overpotentials. They also attributed the low CO_2 selectivity at higher potentials in Pt catalysts to the fact that C–C bond cleavage is inhibited by the presence of surface oxidants. This

effect can not be observed in our model, where the hydroxyl groups are mainly attached to the secondary metal sites, since water activation into the Pt-sites does not occur at the overpotential range considered here [34–36].

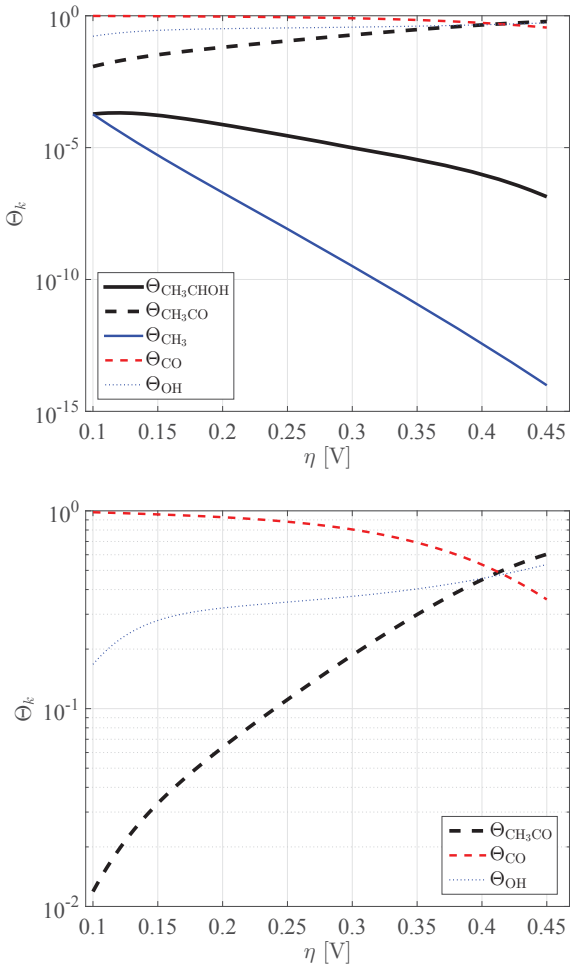

Figure 7: Coverage factors of the five adsorbed species involved in the model plotted as a function of anode overpotential (top) and detail representing only the three largest coverage factors (bottom). Calculation performed with the set of reactions constants optimized to fit Li & Pickup's [16] overpotential and product selectivity data.

Water activation is required, in particular, for Reactions 4, 6 and 7. As seen in Figure 6, the water consumption rate is lower than the ethanol consumption rate both at low and high current densities, the ranges where acetaldehyde selectivity is higher. There is only a narrow gap in the middle, with the lowest acetaldehyde selectivities, where water consumption is sightly higher than ethanol consumption. As indicated by the stoichiometry of the global reactions, water consumption is required for the production of acetic acid, CO_2 and CH_4 through reactions (GR2), (GR3) and (GR4), but not for the production

of acetaldehyde through reaction (GR1), which explains the relation between water consumption and acetaldehyde selectivity.

Figures 8a and 8b show the percentage of the total current density generated by the elementary reactions involving electron transfer. It is seen that the reactions that lead to the formation of adsorbed acetyl (Reactions I, II, III, 1 and 2) generate between 70% and 75% of the total current density. The new path considered in this work (Reactions I, II and III) dominates at low current densities while the original path proposed by Meyer et al. [18] (Reactions 1 and 2) dominates at higher currents. This is compatible with the low acetaldehyde selectivities observed at low-to-medium current densities. Reaction 3 plays also a key role, since it generates about 20% of the total current and produces the adsorbed hydroxyl groups required for Reactions 4, 6 and 7 to proceed. The rest of the current is generated by Reactions 6 and 7, which have nearly the same reaction rate (see Figure 5), although the latter generates five times more current because it involves the transfer of five electrons instead of one. Note that Reaction 8 does not contribute to current generation. This is because the model predicts a negligible methane production ($q_8 \ll q_7$) following the lack of methane selectivity reported in the literature [16, 19, 61]. According to Eqs. (15) and (37), the same reaction rates are then obtained for Reactions 5, 6 and 7.

To finish the discussion of results, Figures 8c and 8d show the selectivity of the four global reactions GRj. Due to the negligible methane production predicted by the model, the selectivity of the global reactions is very similar to that of their corresponding product species. The largest selectivity of the second global reaction, leading to the production of acetic acid, agrees well with the effective electron generation number n^{eff}, which is always close to 4.

5. Conclusions

A detailed reaction mechanism has been proposed to describe ethanol electro-oxidation on binary Pt-based catalysts used in Direct Ethanol PEM Fuel Cells. The kinetic model involves five adsorbates (CH_3CHOH_{ads}, CH_3CO_{ads}, CO_{ads}, $CH_{3\,ads}$, and OH) and six free species, including two reactants (water and ethanol) and four product species (acetaldehyde, acetic acid, carbon dioxide, and methane). The model has been coupled to a 1D across-the-channel description of the mass transport processes that take place in the anode of a DEFC. The resulting mathematical problem yields the coverage factors of the adsorbates, the rates of the elemetary reactions, the production/consumption rates of the free species, the cell current density, the product and global reaction selectivities, and the effective electron generation number for given values of the concentrations of ethanol and acetaldehyde at the anode channel, the anode overpotential, the cell temperature, and a particular set of kinetic constants. A new methodology

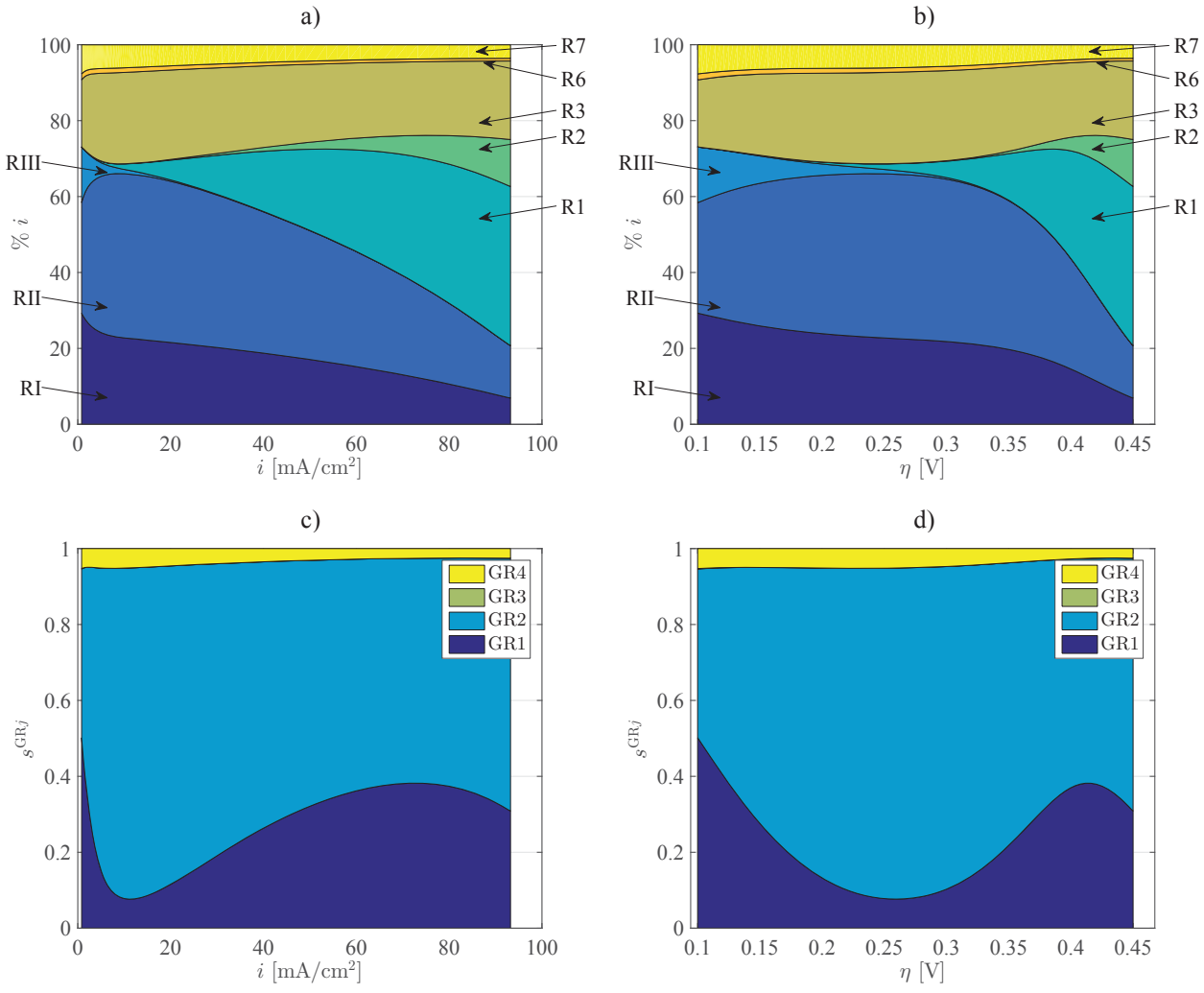

Figure 8: Percentage of the total current density generated by the elementary reactions involving electrons transfer plotted as a function of a) current density and b) anode overpotential, and selectivity of the global reactions GRj, $j = 1, \ldots, 4$, plotted as a function of c) current density and d) anode overpotential. Calculation performed with the set of reactions constants optimized to fit Li & Pickup's [16] overpotential and product selectivity data.

based on the use of a multi-objective genetic algorithm has been used to optimize the set of kinetic constants that better fits selected results taken from the literature. As a result, the genetically optimized model is able to reproduce experimental anode polarization and product selectivity data for all the current densities under study.

Among the chemical species included in the reaction mechanims, the main species involved in current generation are ethanol and acetaldehyde, and the main non-reactive products are acetic acid and CO_2, the concentration of secondary species such as methane being negligibly small. The computation of the global reaction selectivities and the effective electron generation number n^{eff}, introduced for the first

time in this work, showed that the EOR produces roughly 4 electrons in the binary Pt-based catalyst compositions used in state-of-the-art DEFCs. This explains why previous EOR models with acetic acid as unique final product yielded good results in terms of polarization curves. However, they were unable to predict product selectivity.

The proposed 1D across-the-chanel model could be extended to account for the remaining layers of the MEA, namely the cathode catalyst layer (ccl) and the cathode gas diffusion layer (cgdl). The resulting full MEA model (including the agdl, acl, mem, ccl, and cgdl, where mass/charge fluxes are dominated by transverse gradients in the through-plane direction) could be coupled to a 1D along-the-channel model (including the anode and cathode channels, where mass transport fluxes are dominated by downstream convection) to yield a fully predictive 1D+1D operational model for DEFCs. However, introducing such complexity at this early stage of development was considered counterproductive for our main goal of optimizing the multi-step EOR mechanism. As a result, such extensions are left for future work.

The influence of mass transport also warrants further work. The fibrous nature of the GDL combined with the cell assembly process are known to modify the effective mass transport properties. Effective diffusivities derived from detailed studies of fibrous porous layers [57, 58] may be used to improve the values of the kinetic constants reported herein. The methodology described in this work could also be used to investigate the kinetics of the EOR on different catalyst layers, provided overpotential and product selectivity data were available.

Acknowledgments

This work has been partially supported by Projects ENE2011-24574 and ENE2015-68703-C2-1-R (MINECO/FEDER, UE). We would like to thank Dr. José J. Linares for his initial suggestion to work on this problem, and Dr. J. Gómez-Hernandez for helpful comments and discussions.

Nomenclature

Symbols

$C_{k,\ell}$	molar concentration of species k in layer ℓ [mol m^{-3}]
$D_{k,\ell}$	molecular diffusivity of species k in layer ℓ [m^2 s^{-1}]
F	Faraday's constant, 96487 [C mol^{-1}]
h	mass transport coefficient ac/agdl [m s^{-1}]
i	current density [A m^{-2}]
k_r	rate constant of Reaction r [mol m^{-3} s^{-1}] or [s^{-1}]
n^{eff}	effective electron generation number
n_d^k	electroosmotic drag coefficient of species k
N_k	molar flux of species k [mol m^{-2} s^{-1}]
q_r	net reaction rate of Reaction r [mol m^{-3} s^{-1}]
R	ideal-gas constant, 8.3143 [J mol^{-1} K^{-1}]
s_k	selectivity of product species k
s^{GRj}	selectivity of global reaction GRj
T	Temperature [K]
v_{W}	drag velocity of water in the anode gdl [m s−1]
W	molar mass [kg mol^{-1}]
y	coordinate across the membrane

Greek letters

α_r	charge transfer coefficient of Reaction r [-]
δ_ℓ	thickness of layer ℓ [μ m]
ϵ	gdl porosity [-]
η	overpotential [V]
Θ_k	coverage factor of adsorbed species k [-]
ρ	fluid density [kg m^{-3}]
ω_k	net molar production rate of free species k [mol m^{-2} s^{-1}]

Subscripts

a	anode
ac	anode channel

acl	anode catalyst layer
agdl	anode gas diffusion layer
ads	adsorbed
A	acetaldehyde (CH_3CHO)
AA	acetic acid (CH_3COOH)
ccl	cathode catalyst layer
cross	crossover flux
E	ethanol (CH_3CH_2OH)
k	species k
ℓ	generic layer
r	reaction r
W	water (H_2O)

Superscripts

eff	effective property

Bibliography

[1] C. Lamy, A. Lima, V. LeRhun, F. Delime, C. Coutanceau, J.-M. Léger, Recent advances in the development of direct alcohol fuel cells (DAFC), J. Power Sources 105 (2) (2002) 283–296.
URL http://www.sciencedirect.com/science/article/pii/S0378775301009545

[2] J. Friedl, U. Stimming, Model catalyst studies on hydrogen and ethanol oxidation for fuel cells, Electrochim. Acta 101 (2013) 41–58.
URL http://www.sciencedirect.com/science/article/pii/S0013468613000108

[3] M. Z. F. Kamarudin, S. K. Kamarudin, M. S. Masdar, W. R. W. Daud, Review: Direct ethanol fuel cells, Int. J. Hydrogen Energy 38 (22) (2013) 9438–9453.
URL http://www.sciencedirect.com/science/article/pii/S0360319912016369

[4] A. Brouzgou, A. K. M. Podias, P. Tsiakaras, PEMFCs and AEMFCs directly fed with ethanol: A current status comparative review, J. Appl. Electrochem. 43 (2) (2013) 119–136.
URL http://link.springer.com/10.1007/s10800-012-0513-2

[5] S. Song, P. Tsiakaras, Recent progress in direct ethanol proton exchange membrane fuel cells (DE-PEMFCs), Appl. Catal. B Environ. 63 (3) (2006) 187–193.

[6] J. Wang, S. Wasmus, R. F. Savinell, Evaluation of Ethanol, 1-Propanol, and 2-Propanol in a Direct Oxidation Polymer-Electrolyte Fuel Cell, J. Electrochem. Soc. 142 (12) (1995) 4218.
URL http://jes.ecsdl.org/cgi/doi/10.1149/1.2048487

[7] S. Song, W. Zhou, Z. Liang, R. Cai, G. Sun, Q. Xin, V. Stergiopoulos, P. Tsiakaras, The effect of methanol and ethanol cross-over on the performance of PtRu/C-based anode DAFCs, Appl. Catal. B Environ. 55 (1) (2005) 65–72.

[8] P. Ekdharmasuit, A. Therdthianwong, S. Therdthianwong, Anode structure design for generating high stable power output for direct ethanol fuel cells, Fuel 113 (2013) 69–76.
URL http://www.sciencedirect.com/science/article/pii/S0016236113004584

[9] J. Goldemberg, S. T. Coelho, P. M. Nastari, O. Lucon, Ethanol learning curveâthe Brazilian experience, Biomass and Bioenergy 26 (3) (2004) 301–304.

[10] H. Hitmi, E. M. Belgsir, J.-M. Léger, C. Lamy, R. O. Lezna, A kinetic analysis of the electro-oxidation of ethanol at a platinum electrode in acid medium, Electrochim. Acta 39 (3) (1994)

407–415.
URL http://www.sciencedirect.com/science/article/pii/0013468694800804

[11] T. Iwasita, E. Pastor, A dems and FTir spectroscopic investigation of adsorbed ethanol on polycrystalline platinum, Electrochim. Acta 39 (4) (1994) 531–537.

[12] H. Wang, Z. Jusys, R. J. Behm, Ethanol electro-oxidation on carbon-supported Pt, PtRu and Pt3Sn catalysts: A quantitative DEMS study, J. Power Sources 154 (2) (2006) 351–359.
URL http://linkinghub.elsevier.com/retrieve/pii/S0378775305014333
http://www.sciencedirect.com/science/article/pii/S0378775305014333

[13] H. Wang, Z. Jusys, R. J. Behm, Ethanol Electrooxidation on a Carbon-Supported Pt Catalyst: Reaction Kinetics and Product Yields, J. Phys. Chem. B 108 (50) (2004) 19413–19424.
URL http://dx.doi.org/10.1021/jp046561k

[14] J.-M. Léger, S. Rousseau, C. Coutanceau, F. Hahn, C. Lamy, How bimetallic electrocatalysts does work for reactions involved in fuel cells?: Example of ethanol oxidation and comparison to methanol, Electrochim. Acta 50 (25) (2005) 5118–5125.

[15] M. H. Shao, R. R. Adzic, Electrooxidation of ethanol on a Pt electrode in acid solutions: in situ ATR-SEIRAS study, Electrochim. Acta 50 (12) (2005) 2415–2422.

[16] G. Li, P. G. Pickup, Analysis of performance losses of direct ethanol fuel cells with the aid of a reference electrode, J. Power Sources 161 (1) (2006) 256–263.
URL http://linkinghub.elsevier.com/retrieve/pii/S0378775306005945

[17] E. Antolini, Catalysts for direct ethanol fuel cells, J. Power Sources 170 (1) (2007) 1–12.
URL http://www.sciencedirect.com/science/article/pii/S0378775307007161
http://linkinghub.elsevier.com/retrieve/pii/S0378775307007161

[18] M. Meyer, J. Melke, D. Gerteisen, Modelling and simulation of a direct ethanol fuel cell considering multistep electrochemical reactions, transport processes and mixed potentials, Electrochim. Acta 56 (11) (2011) 4299–4307.
URL http://www.sciencedirect.com/science/article/pii/S0013468611001319

[19] R. M. Antoniassi, A. Oliveira Neto, M. Linardi, E. V. Spinacé, The effect of acetaldehyde and acetic acid on the direct ethanol fuel cell performance using PtSnO2/C electrocatalysts, Int. J. Hydrogen

Energy 38 (27) (2013) 12069–12077.
URL http://linkinghub.elsevier.com/retrieve/pii/S0360319913016704

[20] I. Kim, O. H. Han, S. A. Chae, Y. Paik, S.-H. Kwon, K.-S. Lee, Y.-E. Sung, H. Kim, Catalytic reactions in direct ethanol fuel cells., Angew. Chem. Int. Ed. Engl. 50 (10) (2011) 2270–4.
URL http://www.ncbi.nlm.nih.gov/pubmed/21351334

[21] K. Taneda, Y. Yamazaki, Study of direct type ethanol fuel cells, Electrochim. Acta 52 (4) (2006) 1627–1631.
URL http://ac.els-cdn.com/S0013468606003987/1-s2.0-S0013468606003987-main.pdf?_tid=dba478
http://www.sciencedirect.com/science/article/pii/S0013468606003987

[22] A. Jablonski, P. J. Kulesza, A. Lewera, Oxygen permeation through Nafion 117 membrane and its impact on efficiency of polymer membrane ethanol fuel cell, J. Power Sources 196 (10) (2011) 4714–4718.
URL http://linkinghub.elsevier.com/retrieve/pii/S0378775311001571

[23] R. A. Rightmire, R. L. Rowland, D. L. Boos, D. L. Beals, Ethyl Alcohol Oxidation at Platinum Electrodes, J. Electrochem. Soc. 111 (2) (1964) 242.
URL http://jes.ecsdl.org/cgi/doi/10.1149/1.2426092

[24] H.-F. Wang, Z.-P. Liu, Comprehensive mechanism and structure-sensitivity of ethanol oxidation on platinum: new transition-state searching method for resolving the complex reaction network., J. Am. Chem. Soc. 130 (33) (2008) 10996–1004.
URL http://dx.doi.org/10.1021/ja801648h

[25] R. Kavanagh, X. M. Cao, W. F. Lin, C. Hardacre, P. Hu, Origin of low CO$_2$ selectivity on platinum in the direct ethanol fuel cell., Angew. Chem. Int. Ed. Engl. 51 (7) (2012) 1572–5.
URL https://www.ncbi.nlm.nih.gov/pmc/articles/PMC3625737

[26] M. A. F. Akhairi, S. K. Kamarudin, Catalysts in direct ethanol fuel cell (DEFC): An overview, Int. J. Hydrogen Energy 41 (7) (2016) 4214–4228.
URL http://linkinghub.elsevier.com/retrieve/pii/S0360319915027846

[27] F. Vigier, C. Coutanceau, F. Hahn, E. M. Belgsir, C. Lamy, On the mechanism of ethanol electro-oxidation on Pt and PtSn catalysts: electrochemical and in situ IR reflectance spectroscopy studies,

J. Electroanal. Chem. 563 (1) (2004) 81–89.
URL http://www.sciencedirect.com/science/article/pii/S0022072803005175

[28] S. Rousseau, C. Coutanceau, C. Lamy, J.-M. Léger, Direct ethanol fuel cell (DEFC): Electrical performances and reaction products distribution under operating conditions with different platinum-based anodes, J. Power Sources 158 (1) (2006) 18–24.
URL http://www.sciencedirect.com/science/article/pii/S0378775305012024 http://linkinghub.elsevier.com/retrieve/pii/S0378775305012024

[29] F. Colmati, E. Antolini, E. R. Gonzalez, Effect of temperature on the mechanism of ethanol oxidation on carbon supported Pt, PtRu and Pt$_3$Sn electrocatalysts, J. Power Sources 157 (1) (2006) 98–103.

[30] H. Li, G. Sun, L. Cao, L. Jiang, Q. Xin, Comparison of different promotion effect of PtRu/C and PtSn/C electrocatalysts for ethanol electro-oxidation, Electrochim. Acta 52 (24) (2007) 6622–6629.

[31] K. Fatih, V. Neburchilov, V. Alzate, R. Neagu, H. Wang, Synthesis and characterization of quaternary PtRuIrSn/C electrocatalysts for direct ethanol fuel cells, J. Power Sources 195 (21) (2010) 7168–7175.

[32] A. Bach Delpeuch, F. Maillard, M. Chatenet, P. Soudant, C. Cremers, Ethanol oxidation reaction (EOR) investigation on Pt/C, Rh/C, and Pt-based bi- and tri-metallic electrocatalysts: A DEMS and in situ FTIR study, Appl. Catal. B Environ. 181 (2016) 672–680.
URL http://www.sciencedirect.com/science/article/pii/S0926337315301144 http://linkinghub.elsevier.com/retrieve/pii/S0926337315301144

[33] P. J. Kulesza, I. S. Pieta, I. A. Rutkowska, A. Wadas, D. Marks, K. Klak, L. Stobinski, J. A. Cox, Electrocatalytic oxidation of small organic molecules in acid medium: Enhancement of activity of noble metal nanoparticles and their alloys by supporting or modifying them with metal oxides, Electrochim. Acta 110 (2013) 474–483.
URL http://dx.doi.org/10.1016/j.electacta.2013.06.052

[34] M. Watanabe, S. Motoo, Electrocatalysis by ad-atoms, J. Electroanal. Chem. Interfacial Electrochem. 60 (3) (1975) 275–283.
URL http://www.sciencedirect.com/science/article/pii/S0022072875802622

[35] F. Vigier, C. Coutanceau, A. Perrard, E. M. Belgsir, C. Lamy, Development of anode catalysts for a direct ethanol fuel cell, J. Appl. Electrochem. 34 (4) (2004) 439–446.
URL http://link.springer.com/10.1023/B:JACH.0000016629.98535.ad

[36] F. Vigier, S. Rousseau, C. Coutanceau, J.-M. Leger, C. Lamy, Electrocatalysis for the direct alcohol fuel cell, Top. Catal. 40 (1-4) (2006) 111–121.
URL http://link.springer.com/10.1007/s11244-006-0113-7

[37] S. Song, G. Wang, W. Zhou, X. Zhao, G. Sun, Q. Xin, S. Kontou, P. Tsiakaras, The effect of the MEA preparation procedure on both ethanol crossover and DEFC performance, J. Power Sources 140 (1) (2005) 103–110.

[38] D. D. James, P. G. Pickup, Effects of crossover on product yields measured for direct ethanol fuel cells, Electrochim. Acta 55 (11) (2010) 3824–3829.
URL http://linkinghub.elsevier.com/retrieve/pii/S0013468610002161

[39] Z. Zakaria, S. K. Kamarudin, S. N. Timmiati, Membranes for direct ethanol fuel cells: An overview, Appl. Energy 163 (2016) 334–342.
URL http://linkinghub.elsevier.com/retrieve/pii/S0306261915013641

[40] G. M. Andreadis, S. Song, P. E. Tsiakaras, Direct ethanol fuel cell anode simulation model, J. Power Sources 157 (2) (2006) 657–665.
URL http://linkinghub.elsevier.com/retrieve/pii/S0378775306000140

[41] G. M. Andreadis, P. E. Tsiakaras, Ethanol crossover and direct ethanol PEM fuel cell performance modeling and experimental validation, Chem. Eng. Sci. 61 (22) (2006) 7497–7508.
URL http://www.sciencedirect.com/science/article/pii/S0009250906005197

[42] G. M. Andreadis, A. K. M. Podias, P. E. Tsiakaras, The effect of the parasitic current on the Direct Ethanol PEM Fuel Cell Operation, J. Power Sources 181 (2) (2008) 214–227.
URL http://linkinghub.elsevier.com/retrieve/pii/S0378775308001857

[43] G. M. Andreadis, A. K. M. Podias, P. E. Tsiakaras, A model-based parametric analysis of a direct ethanol polymer electrolyte membrane fuel cell performance, J. Power Sources 194 (1) (2009) 397–407.
URL http://linkinghub.elsevier.com/retrieve/pii/S0378775309007782

[44] S. Lin Ee, E. Birgersson, Two-Dimensional Approximate Analytical Solutions for the Direct Liquid Fuel Cell, J. Electrochem. Soc. 158 (10) (2011) B1224.
URL http://jes.ecsdl.org/cgi/doi/10.1149/1.3621950

[45] H. Pramanik, S. Basu, Modeling and experimental validation of overpotentials of a direct ethanol fuel cell, Chem. Eng. Process. Process Intensif. 49 (7) (2010) 635–642.

[46] R. Sousa, D. M. dos Anjos, G. Tremiliosi-Filho, E. R. Gonzalez, C. Coutanceau, E. Sibert, J.-M. Léger, K. B. Kokoh, Modeling and simulation of the anode in direct ethanol fuels cells, J. Power Sources 180 (1) (2008) 283–293.

[47] P. S. Kauranen, E. Skou, J. Munk, Kinetics of methanol oxidation on carbon-supported Pt and Pt + Ru catalysts, J. Electroanal. Chem. 404 (1) (1996) 1–13.

[48] K. Sundmacher, T. Schultz, S. Zhou, K. Scott, M. Ginkel, E. D. Gilles, Dynamics of the direct methanol fuel cell (DMFC): experiments and model-based analysis, Chem. Eng. Sci. 56 (2) (2001) 333–341.

[49] M. R. Shivhare, C. L. Jackson, K. Scott, E. B. Martin, Simplified model for the direct methanol fuel cell anode, J. Power Sources 173 (1) (2007) 240–248.

[50] M. R. Shivhare, R. G. Allen, K. Scott, A. J. Morris, E. B. Martin, A kinetic model for the direct methanol fuel cell anode based on surface coverage, J. Electroanal. Chem. 595 (2) (2006) 145–151.

[51] N. Suresh, S. Jayanti, Cross-over and performance modeling of liquid-feed Polymer Electrolyte Membrane Direct Ethanol Fuel Cells, Int. J. Hydrogen Energy 36 (22) (2011) 14648–14658.

[52] J. Sanchez-Monreal, P. A. García-Salaberri, M. Vera, Mathematical Modeling of Direct Ethanol Fuel Cells Using a Multi-Step Chemical Kinetic Mechanism, ECS Trans. 72 (25) (2016) 1–16.
URL http://ecst.ecsdl.org/cgi/doi/10.1149/07225.0001ecst

[53] M. Vera, A single-phase model for liquid-feed DMFCs with non-Tafel kinetics, J. Power Sources 171 (2) (2007) 763–777.

[54] R. B. Kutz, B. Braunschweig, P. Mukherjee, R. L. Behrens, D. D. Dlott, A. Wieckowski, Reaction pathways of ethanol electrooxidation on polycrystalline platinum catalysts in acidic electrolytes, J. Catal. 278 (2) (2011) 181–188.

[55] A. A. Abd-El-Latif, E. Mostafa, S. Huxter, G. Attard, H. Baltruschat, Electrooxidation of ethanol at polycrystalline and platinum stepped single crystals: A study by differential electrochemical mass spectrometry, Electrochim. Acta 55 (27) (2010) 7951–7960.

[56] M. J. Giz, G. A. Camara, The ethanol electrooxidation reaction at Pt (111): The effect of ethanol concentration, J. Electroanal. Chem. 625 (2) (2009) 117–122.

[57] P. A. García-Salaberri, G. Hwang, M. Vera, A. Z. Weber, J. T. Gostick, Effective diffusivity in partially-saturated carbon-fiber gas diffusion layers: Effect of through-plane saturation distribution, Int. J. Heat Mass Transf. 86 (2015) 319–333.
URL http://linkinghub.elsevier.com/retrieve/pii/S001793101500246X

[58] P. A. García-Salaberri, J. T. Gostick, G. Hwang, A. Z. Weber, M. Vera, Effective diffusivity in partially-saturated carbon-fiber gas diffusion layers: Effect of local saturation and application to macroscopic continuum models, J. Power Sources 296 (2015) 440–453.
URL http://linkinghub.elsevier.com/retrieve/pii/S0378775315300823

[59] P. A. García-Salaberri, M. Vera, R. Zaera, Nonlinear orthotropic model of the inhomogeneous assembly compression of PEM fuel cell gas diffusion layers, Int. J. Hydrogen Energy 36 (18) (2011) 11856–11870.
URL http://linkinghub.elsevier.com/retrieve/pii/S0360319911014017

[60] H. Guo, C.-F. Ma, 2D analytical model of a direct methanol fuel cell, Electrochem. commun. 6 (3) (2004) 306–312.

[61] G. M. Andreadis, V. Stergiopoulos, S. Song, P. E. Tsiakaras, Direct ethanol fuel cells: The effect of the cell discharge current on the products distribution, Appl. Catal. B Environ. 100 (1-2) (2010) 157–164.
URL http://linkinghub.elsevier.com/retrieve/pii/S0926337310003310

[62] D. R. Lide, Handbook of Chemistry and Physics, CRC Press, Boca Raton, 1990.

Appendix A. Solution for the coverage factors

The coverage factors of the five adsorbates (CH_3CHOH_{ads}, CH_3CO_{ads}, CO_{ads}, $CH_{3\,ads}$, and OH_{ads}) are determined by the system of non-linear algebraic equations (12)–(16)

$$\Theta_{CH_3CHOH}: \quad q_{\rm I} - q_{\rm II} - q_{\rm III} = 0 \tag{12}$$

$$\Theta_{CH_3CO}: \quad q_2 + q_{\rm II} - q_5 - q_4 = 0 \tag{13}$$

$$\Theta_{OH}: \quad q_3 - q_4 - q_6 - 2q_7 = 0 \tag{14}$$

$$\Theta_{CO}: \quad q_5 - q_6 = 0 \tag{15}$$

$$\Theta_{CH_3}: \quad q_5 - q_8 - q_7 = 0 \tag{16}$$

This non-linear system, which can not be solved analytically, may have multiple solutions, including complex ones. To avoid non-physical solutions the system can be reduced to a fifth-order polynomial equation for $\Theta_{OH_{ads}}$ which must have at least one real root between 0 and 1.

In order to simplify the algebraic expressions, the following notation will be used for the rate constants of the reactions involving electrons transfer

$$\mathfrak{K}_{\rm rf} = k_{\rm rf} \exp\left(\frac{\alpha_{\rm r} nF}{RT}\eta_a\right), \quad \mathfrak{K}_{\rm rb} = k_{\rm rb} \exp\left(-\frac{(1-\alpha_{\rm r})nF}{RT}\eta_a\right) \tag{A.1}$$

Introducing expressions (1)–(11) for the reaction rates in Eqs. (12)–(16) leads to the following set of equations for the coverage factors

$$\begin{aligned}(1 - \Theta_{CH_3CHOH} - \Theta_{CH_3CO} - \Theta_{CO} - \Theta_{CH_3})\, C_{\rm E,acl}\mathfrak{K}_{\rm If} \\ - \Theta_{CH_3CHOH}\mathfrak{K}_{\rm Ib} - \Theta_{CH_3CHOH}\mathfrak{K}_{\rm IIf} + \Theta_{CH_3CO}\mathfrak{K}_{\rm IIb} - \Theta_{CH_3CHOH}\mathfrak{K}_{\rm IIIf} \\ + (1 - \Theta_{CH_3CHOH} - \Theta_{CH_3CO} - \Theta_{CO} - \Theta_{CH_3})\, C_{\rm A,acl}\mathfrak{K}_{\rm IIIb} = 0\end{aligned} \tag{12'}$$

$$\begin{aligned}(1 - \Theta_{CH_3CHOH} - \Theta_{CH_3CO} - \Theta_{CO} - \Theta_{CH_3})\, C_{\rm A,acl}\mathfrak{K}_{\rm 2f} - \Theta_{CH_3CO}\mathfrak{K}_{\rm 2b} \\ + \Theta_{CH_3CHOH}\mathfrak{K}_{\rm IIf} - \Theta_{CH_3CO}\mathfrak{K}_{\rm IIb} - \Theta_{CH_3CO}\Theta_{OH}k_4 - \Theta_{CH_3CO}k_5 = 0\end{aligned} \tag{13'}$$

$$\begin{aligned}(1 - \Theta_{OH})\,\mathfrak{K}_{\rm 3f} - \Theta_{OH}\mathfrak{K}_{\rm 3b} - \Theta_{CH_3CO}\Theta_{OH}k_4 - \Theta_{CO}\Theta_{OH}\mathfrak{K}_6 \\ - 2\Theta_{CH_3}\Theta_{OH}^2\mathfrak{K}_7 = 0\end{aligned} \tag{14'}$$

$$\Theta_{CH_3CO} k_5 - \Theta_{CH_3} \Theta_{OH}^2 \Re_7 - \Theta_{CH_3} \Re_8 = 0 \tag{15'}$$

$$\Theta_{CH_3CO} k_5 - \Theta_{CO} \Theta_{OH} \Re_6 = 0 \tag{16'}$$

Converting this system of equations into a single polinomial equation for $\Theta_{OH_{ads}}$ requires a series of algebraic manipulations. First, Eq. (15') must be rewritten as

$$\Theta_{CH_3CO} = \frac{\Theta_{CH_3} \left(\Re_7 \Theta_{OH}^2 + \Re_8 \right)}{k_5} \tag{A.2}$$

Substituting this expression in (16') leads to

$$\Theta_{CO} = \frac{\Theta_{CH_3} \left(\Re_7 \Theta_{OH}^2 + \Re_8 \right)}{\Re_6 \Theta_{OH}} \tag{A.3}$$

And using (A.2) and (A.3) in Eq. (12') gives

$$\Theta_{CH_3CHOH} = \left(1 - \frac{\Theta_{CH_3} \left(\Re_7 \Theta_{OH}^2 + \Re_8 \right)}{\Re_6 \Theta_{OH}} - \Theta_{CH_3} \right) \chi_1 - \left(\frac{\Theta_{CH_3} \left(\Re_7 \Theta_{OH}^2 + \Re_8 \right)}{k_5} \right) \chi_2 \tag{A.4}$$

with

$$\chi_1 = \frac{C_{E,acl} \Re_{If} + C_{A,acl} \Re_{IIIb}}{C_{E,acl} \Re_{If} + C_{A,acl} \Re_{IIIb} + \Re_{Ib} + \Re_{IIf} + \Re_{IIIf}} \tag{A.5}$$

$$\chi_2 = \frac{C_{E,acl} \Re_{If} + C_{A,acl} \Re_{IIIb} - \Re_{IIb}}{C_{E,acl} \Re_{If} + C_{A,acl} \Re_{IIIb} + \Re_{Ib} + \Re_{IIf} + \Re_{IIIf}} \tag{A.6}$$

Substituting now (A.2), (A.3), and (A.4) in Eq. (13') provides Θ_{CH_3} in terms of Θ_{OH} as follows

$$\Theta_{CH_3} = \frac{C_{A,acl} \Re_{2f} + \left(\Re_{IIf} - C_{A,acl} \Re_{2f} \right) \chi_1}{\beta_{-1} \Theta_{OH}^{-1} + \beta_0 + \beta_1 \Theta_{OH} + \beta_2 \Theta_{OH}^2 + \beta_3 \Theta_{OH}^3} \tag{A.7}$$

with

$$\beta_{-1} = C_{A,acl} \Re_{2f} \frac{\Re_8}{\Re_6} + \left(\Re_{IIf} - C_{A,acl} \Re_{2f} \right) \chi_1 \frac{\Re_8}{\Re_6} \tag{A.8}$$

$$\beta_0 = -C_{A,acl} \Re_{2f} - \left(C_{A,acl} \Re_{2f} + \Re_{2b} + k_5 \right) \frac{\Re_8}{k_5} + \left(C_{A,acl} \Re_{2f} - \Re_{IIf} \right) \left(\chi_1 + \chi_2 \frac{\Re_8}{k_5} \right) - \Re_{IIb} \frac{\Re_8}{k_5} \tag{A.9}$$

$$\beta_1 = \frac{C_{A,acl} \Re_{2f} \Re_7}{k_5} + \frac{k_4 \Re_8}{k_5} + \chi_1 \frac{\Re_7}{\Re_6} \left(\Re_{IIf} - C_{A,acl} \Re_{2f} \right) \tag{A.10}$$

$$\beta_2 = \left(C_{A,acl} \Re_{2f} + \Re_{2b} + k_5 \right) \frac{\Re_7}{k_5} + \left(\Re_{IIb} + \chi_2 \left(\Re_{IIf} - C_{A,acl} \Re_{2f} \right) \right) \frac{\Re_7}{k_5} \tag{A.11}$$

$$\beta_3 = \frac{k_4 \Re_7}{k_5} \tag{A.12}$$

Moreover, with the aid of (A.2) and (A.3), Eq. (14') can be written exclusively in terms of Θ_{OH} and Θ_{CH_3}, namely

$$1 - \varphi\Theta_{OH} - \left(\eta_0 + \eta_1\Theta_{OH} + \eta_2\Theta_{OH}^2 + \eta_3\Theta_{OH}^3\right)\Theta_{CH_3} = 0 \tag{A.13}$$

where

$$\begin{aligned} \varphi &= 1 + \frac{\mathfrak{K}_{3b}}{\mathfrak{K}_{3f}} \\ \eta_0 = \frac{\mathfrak{K}_8}{\mathfrak{K}_{3f}}, \quad \eta_1 &= \frac{k_4\mathfrak{K}_8}{k_5\mathfrak{K}_{3f}}, \quad \eta_2 = 3\frac{\mathfrak{K}_7}{\mathfrak{K}_{3f}}, \quad \eta_3 = \frac{k_4\mathfrak{K}_7}{k_5\mathfrak{K}_{3f}} \end{aligned} \tag{A.14}$$

Combining Eqs. (A.7) and (A.13), the following equation for $\Theta_{OH_{ads}}$ is finally obtained

$$\begin{aligned} &(\quad + \varphi\beta_3 \quad)\Theta_{OH}^5 \\ &+ (B\eta_3 + \varphi\beta_2 \quad - \beta_3 \;)\Theta_{OH}^4 \\ &+ (B\eta_2 + \varphi\beta_1 \quad - \beta_2 \;)\Theta_{OH}^3 \\ &+ (B\eta_1 + \varphi\beta_0 \quad - \beta_1 \;)\Theta_{OH}^2 \\ &+ (B\eta_0 + \varphi\beta_{-1} - \beta_0 \;)\Theta_{OH} \\ &+ (\qquad\qquad - \beta_{-1}) \qquad = 0 \end{aligned} \tag{A.15}$$

The fact that this is a fifth-order polynomial equation ensures that there is at least one real root of (A.15). Moreover, the positive and negative signs of the highest order coefficient ($\varphi\beta_3$) and the independent term ($-\beta_{-1}$) guarantee that this root is positive. In order to be physically meaningful, it must be checked that the value of Θ_{OH} thus obtained lies between 0 and 1.